

**Republic of Iraq
Ministry of Higher Education & Scientific Research
University of Baghdad College of Education for Pure
Science / Ibn Al-Haitham**



Amorphous silicon Light Emitting Diode Quantum Dots

A Thesis

**Submitted to University of Baghdad College of Education
for Pure Science / Ibn Al-Haitham in Partial Fulfillment
Of the Requirements for the Degree of Master of
Science (M.Sc.) in Physics**

By

**Walaa Khalel Jameel Khalel
(B.Sc. 2012)**

Supervisor

**Dr. Moafak C. Abdulrida
Assistant Professor**

2015 A.C.

1436 A.H.

بِسْمِ اللَّهِ الرَّحْمَنِ الرَّحِيمِ

إِنْ أَرِيدُ إِلَّا الْإِصْلَاحَ مَا اسْتَطَعْتُ
وَمَا تَوْفِيقِي إِلَّا بِاللَّهِ عَلَيْهِ تَوَكَّلْتُ
وَإِلَيْهِ أُنِيبُ

سورة هود

آية (88)

*I Dedicate it to
My Father,
Mother and my Son
Abdulrahman*

Acknowledgement

First of all, thanks to **ALLAH HIS MAJESTY** for His uncountable Blessings. Special appreciation to my supervisor **Dr. Moafak C. Abdulrida** for suggesting this project and for his support and encouragement over the research work. I express my gratitude to him for assistance, valuable comments and suggestions. I would like to thank him for his wonderful guidance in this research especially his useful and beautiful discussions.

My deepest gratitude is to all the benevolent hands that lend me a help in this project, especially:

- The Head Dr. Kareem Ali Jasim and the staff of Physics Department/ College of Education for pure science/(Ibn Al-Haitham) especially Dr.Ahlam H. Jaffar Al-Mosawi and Dr. Sameer Atta Makki.
- Dr. Nidhal. M. Abduh-Ameer for her useful and important discussions.
- My husband for his support and continuous invocation through my study time.
- All my friends for their encouragement.

Walaa

Abstract

In this work, theoretical calculations were used by considering the amorphous silicon quantum dots light emitting diode (a-SiQDs LED) as the device of investigation. By these calculations, the effect of quantum confinement was analyzed. It is found that the light emission shows significant size dependence in the range (1-4) nm of the quantum dots. The internal quantum efficiency is affected by temperature and it is more efficient at room temperature. The energy gap can be tuned by controlling the size of a-SiQDs. The blue shift is attributed to quantum confinement effect in a-SiQDs structure, where quantum confinements make silicon like candidate for full-color display. It led to the interpretation that the a-SiQDs material has been changed to be a direct band gap material. Internal quantum efficiency as a function of wavelength and injection current has been studied. It is found that the obtained results are in good agreement with the experimental published data. Therefore, a-SiQDs material was asserted to be a promising candidate for visible, tunable and high performance light emitting devices.

Contents

Abstract	I
Acknowledgement	II
The Abbreviations List	III
The Symbol List	IV
The Figure List	VII
Contents	X
Chapter One Basic Concepts	
1.1 Introduction	2
1.2 Amorphous Silicon	4
1.2.1 Optical Properties	6
1.2.1.A Direct and Indirect Transition	6
1.2.1.B Nano Silicon	8
1.2.2 Electrical Conduction	9
1.3 Generation and Recombination	10
1.4 Semiconductor Nanostructure	13
1.4.1 The Classification of of Low-Dimensional Structures	15
1.4.2 The Fabrication Technology	16
1.5 Silicon Quantum Dots System	19
1.5.1 Classification of SiQDs	19
1.5.2 Confinement in Nano Silicon	20
1.6 Light Emitting Diode	20
1.6.1 HeteroStructure LED	20
1.6.2 Nanostructure LED	23
1.7 Literature Survey	24
1.8 The Aim of Present Work	25
Chapter Two Theory and Calculations	
2.1 Introduction	26
2.2 Nano LED	28
2.2.1 Structure of doped Nano LED	28
2.2.2 QDs LED	31
2.2.3 Electrical Properties of LED	32
2.3 Amorphous Silicon Quantum Dots as Light Emitter	33
2.4 The Density of States	33

2.5	Delta Function	36
2.6	LED Efficiency	37
2.6.1	Internal Quantum Efficiency	37
2.6.2	Extraction and External Efficiency	39
2.7	The Main Parameters of a-Si	40
2.8	The Calculations	40
2.8.1	Current-Voltage (I-V) Characteristics	40
2.8.2	The Fitting Current-Voltage (I-V) curve	41
Chapter Three Results, Discussion and Conclusions		
3.1	Introduction	44
3.2	Internal Quantum Efficiency as a Function of Wavelength	44
3.2.1	The Effect of Recombination Lifetime	44
3.2.2	The Effect of Temperature	46
3.3	Internal Efficiency as a Function of Injection Current	42
3.3.1	The Effect of Temperature at Dot Size 1.8 nm	42
3.3.2	The Effect of Quantum Dot Size	50
3.3.3	The Effect of Temperature	51
3.3.4	Constant Dot Size and Temperature with Different Lifetime	53
3.4	The Effect of Quantum Dot Size on Internal Quantum Efficiency	54
3.5	General Discussion	55
3.5.1	Internal Quantum Efficiency as a Function of Wavelength	55
3.5.2	Internal Quantum Efficiency as a Function of Injection Current	56
3.6	Conclusions	59
3.7	Suggestions for Future Work	60
	Reference	61
	Appendices	72

The Figure List

Figure	Page
Fig. (1-1): Structure of hydrogenated amorphous silicon	5
Fig.(1-2-a) Energy vs. crystal momentum for a Semiconductore with an indirect band gap.	6
Fig.(1-2-b): Energy vs. crystal momentum for a semiconductor with a direct band gap.	7
Fig. (1-3): Carrier recombination mechanisms in semiconductors	9
Fig. (1-4): Carrier generation due to light absorption and ionization due to high-energy particle beams	10
Fig. (1-5): The probabilities of radiative recombination : (a) Delocalized to delocalized states; (b) Delocalized to localized (c) Localized to localized state.	11
Fig. (1-6): Nanostructure techniques which are divided into Top down and bottom up Techniques with their scale	15
Fig. (1-7): (a) Under forward bias of a p-n junction, electrons injected from n-side recombine with holes injected from p-side. (b) Higher carrier densities and improved carrier confinement in a double heterojunction.	18
Fig. (2-1): shows the current-voltage (I-V) characteristics of a-Si QD LEDs with Ni/Au contact annealed at 400 °C in air	24
Fig. (2-2): PL peak energy of a-Si DQs as a function of dot size a-Si QDs	24
Fig. (2-3): The structure of a-Si QD LEDs	25

Fig. (2-4): The Density of states for (a) bulk material (b) 2-D structure (c) 1-D structure (d) 0-D structure	29
Fig. (3-1): The internal quantum efficiency as a function of wavelength at different lifetime.	37
Fig. (3-2): The internal quantum efficiency as a function of wavelength with different lifetime.	38
Fig. (3-3): The internal quantum efficiency as a function of wavelength at constant recombination lifetime.	39
Fig. (3-4): The internal quantum efficiency as a function of wavelength at constant recombination lifetime.	40
Fig. (2-1): shows the current-voltage (I-V) characteristics of a-Si QD LEDs with Ni/Au contact annealed at 400 °C in air	24
Fig. (2-2): PL peak energy of a-Si DQs as a function of dot size a-Si QDs	24
Fig. (2-3): The structure of a-Si QD LEDs	25
Fig. (2-4): The Density of states for (a) bulk material (b) 2-D structure (c) 1-D structure (d) 0-D structure	29
Fig. (3-1): The internal quantum efficiency as a function of wavelength at different lifetime.	37
Fig. (3-2): The internal quantum efficiency as a function of wavelength with different lifetime.	38
Fig. (3-3): The internal quantum efficiency as a function of wavelength at constant recombination lifetime.	39
Fig. (3-4): The internal quantum efficiency as a function of wavelength at constant recombination lifetime.	40

Fig. (3-5): The internal quantum efficiency as a function of injection current at different temperatures with recombination lifetime $11 \cdot 10^{-6}$ sec.	41
Fig. (3-6): The internal quantum efficiency as a function of injection current at different temperatures with recombination nsec40lifetime.	41
Fig.(3-7): internal quantum efficiency as a function of injection current.	42
Fig. (3-8): The internal quantum efficiency as a function of injection current.	43
Fig. (3-9): The internal quantum efficiency as a function of injection current.	44
Fig. (3-10): The internal quantum efficiency as a function of injection current.	44
Fig. (3-11): The internal quantum efficiency as a function of injection current.	45
Fig. (3-12): The internal quantum efficiency as a function of injection current.	46
Fig. (3-13): The internal quantum efficiency versus quantum Dot size.	47
Fig. (3-14): From left to right: (a) the effect of spatial confinement with the decreasing of the dot size. (b) the effect of both spatial and quantum confinement with the decreasing of the dot size	50
Fig. (3-8): The internal quantum efficiency as a function of injection current.	43
Fig. (3-9): The internal quantum efficiency as a function of injection current.	44

The Symbol List

Symbol	Definition	Value	Units
ΔK	Different of wave-factor		cm^{-1}
σ_E	Conductivity		$\Omega^{-1}\text{cm}^{-1}$
E_c	Edge of C.B		33
E_F	Fermi level		eV
T	Temperature degree	300	K
K	Boltzmann constant	8.61	eV/K
E_A	Mobility edges of C.B		eV
E_B	Mobility edges of V.B		eV
W_1	Hopping activation energy		eV
E_t	Deep state		eV
E_{bulk}	Bandgap of energy of bulk silicon	1.56	eV
E^0	Energy of band bottom		
E	Energy		
K_x, K_y, K_z	Wave-vector at x, y and z axis		cm^{-1}
m^*	Effective mass		Kg
N(E)	Density of state		$\text{eV}^{-1}\text{cm}^{-3}$
$\hbar = h/2\pi$	Planck's constant	$6.5821 \cdot 10^{-16}$	eV.sec
e	Electronic charge	$1.6 \cdot 10^{-19}$	Coul
$E_{n1,n2,n3}^0$	Energy of sub band bottom		
η_{inj}	Internal quantum efficiency		–
τ_r	Radiative lifetime		Sec

τ_{nr}	Nonradiative lifetime		Sec
I_{inj}	Injection current		Amp
P_{em}	Emission probability		1\sec
r_{sp}	LED spontaneous emission rate		$eV^{-1}sec^{-1}$
V	Volume		cm^3
V	Applied voltage		Volt
$\eta_{extraction}$	Extraction quantum efficiency		–
$\eta_{external}$	External quantum Efficiency		–
P_{opt}	Optical power		
λ	Wavelength		\AA
$\tau_{n,p}$	Minority carrier lifetime		Sec
N_A	Acceptor impurity concentration		cm^{-3}
N_D	Donor impurity concentration		cm^{-3}
V_D	Diode voltage		Volt
Φ_{ph}	Total photon flux		–
A	Surface area		cm^2
C	Confinement parameter	2.4	$eV cm^2$
$D_{n,p}$	Diffusion constant		$cm^2\sec^{-2}$
$h\nu$	Excitation energy		eV
V	Applied voltage		Volt
$\eta_{extraction}$	Extraction quantum efficiency		–

The Abbreviations list

Symbol	Description
LED	Light Emitting Diode
a-Si	Amorphous Silicon
a-Si:H	Hydrogenated Amorphous Silicon
a-SiQDs Dots	Amorphous Silicon Quantum
0-D	Quantum Dot System
1-D	Quantum Wire System
2-D	Quantum Well System
3-D	Bulk System
MBE	Molecular Beam Epitaxial
MOCVD Deposition	Metal-Organic Chemical Vapor
OLED	Organic Light Emitting Diode
QDLED Dots	Light Emitting Diode Quantum
SiQD	Silicon Quantum Dots
ITO	Indium Tin Oxide
I-V	Current-Voltage characteristics
d	Dot Size
p-Si	Porous Silicon
x,y,z	Orthogonal Directions
LEDs	Light Emitting Device
PL	Photoluminescence

Chapter One

**Basic Concepts
Of
Light Emitting Diode**

1.1 Introduction

The semiconductor light emitting devices can be classified into two basic categories: first light emitting diodes (LEDs) that emit incoherent spontaneous light, and second laser diodes emitting coherent radiation [1]. LEDs are the most widely used semiconductor optoelectronic devices. They have a wide application such as, field starting with simple indicator lamps to optical communication sources, from lighting lamps to elements for large color displays [2]. Comparing to the incandescent lamps, the LEDs are highly compact, reliable and offer a relatively high efficiency, brightness and modulation bandwidth. In the present time, they are often replaced by semiconductor laser diodes. Nevertheless, the production of LEDs is much less complicated and therefore cheaper [3]. In applications where the human eye is exposed to the light beam, in terms of safety and inconvenience of speckle typical for coherent light, the temporal and spatial incoherence of LEDs is more of an advantage [1, 2]. Henry Joseph Round of Marconi Labs was the first who noted that a semiconductor junction would produce light from SiC crystallites already in 1907[3] and was recognized at that time as the discoverer of the phenomenon of electroluminescence. Also, Russian Oleg Vladimirovich Losev independently observed luminescence with SiC metal-semiconductor rectifiers [3, 5] and his name has been connected with the invention of the first LED.

Rubin Braunstein of the Radio Corporation of America reported on infrared emission from the gallium arsenide (GaAs) material and other semiconductor alloys in 1955 [4]. Biard and Pittman found in 1961 that gallium arsenide (GaAs) gave an infrared radiation when electric current was applied [3, 6]. They got the patent for the infrared LED Texas Instruments marketed the first commercial LED product. In 1962 Nick Holonyak Jr. presented a method to synthesize gallium arsenide phosphide (GaAsP) crystals [3], which exhibited wavelengths in the visible spectrum. By using this tunable alloy, Holonyak crafted the first practical LED in 1962 (the red LED) and is seen as the father of the light-emitting diode. The Weak band-to-band emission from Si was first observed by Hayness and Briggs [3] using visible light excitation or by forward biasing Si diodes already in 1952. In 1960s, Ralph Logan and his coworkers have pioneered on investigation of indirect band-gap GaP and GaAsP LEDs doped with optically active isoelectronic impurities (nitrogen) [2]. They developed a manufacturing process for production GaP-based red and green LEDs. In the same time, Maruska was working on the investigation of GaN films. In 1969 Maruska succeeded to produce the first single-crystal GaN and in the early 1970s Pankove published a metal (In surface contact) - insulator (Zn doped n-GaN) – semiconductor (p-GaN) diode, which was the first current-injected GaN green and blue (475 nm) light emitter [4].

After two years, Maruska has developed Mg-doped GaN MIS device emitting violet luminescence [4]. In 1990s, Shuji Nakamura demonstrated the first high-brightness blue LED based on GaInN. He proposed that blue LEDs in combination with phosphor coating (yellow light) produce light that appears white. Nakamura was awarded the 2006 Millennium Technology Prize for his invention of blue, green and white light emitting diodes (LEDs) and the blue laser diode [7]. With this wide variety of colors, arrays of multicolor LEDs can be designed to produce unconventional color patterns [8]. In 2014, The Noble prize in physics honours the inventors of blue LED leading to a new generation of bright and energy-efficient white light. This chapter starts with introduction of amorphous silicon, then, it deals with some details the density of state and the optical and electrical properties of amorphous silicon. In fact, this step is necessary to get a rather complete picture of amorphous silicon. Classification of semiconductor nanostructure and technology, and more details of Si-QDs system have been explained. Finally, the concept of heterostructure and nanostructure of light emitting diode are presented.

1.2 Amorphous Silicon

The amorphous silicon (a-Si) was first investigated in 1970 [9]. The amorphous-Si is used in devices typically deposited by plasma – enhanced chemical vapor deposition

from silene at ~ 300 °C as the substrate temperature. Although a-Si has no long range order like a crystal, in device – grade a-Si most silicon atoms still have bonds to four neighboring silicon atoms (Fig. 1.1) [9]. These bonds have a bond length and an angle between bonds close to those in crystalline silicon, despite the lack of long-range order. About 10% of the silicon orbitals do not form bonds with other silicon atoms, but nearly all of these form bonds to hydrogen atom, which reduce the density of residual dangling bonds and states in the band gap to $\sim 10^{16} \text{ cm}^{-3}$ [10]. Since, the material contains on the order of 10% hydrogen, it is often referred to as "hydrogenated amorphous silicon", a-si:H, because the bond lengths and angles are not all ideal, many of the bonds are strained [11]. As a result, the edges of the conduction and valence band are not sharp, and the states at the edges of the conduction and valence bands closest to midgap are not conventional conduction states, but rather localized states [9].

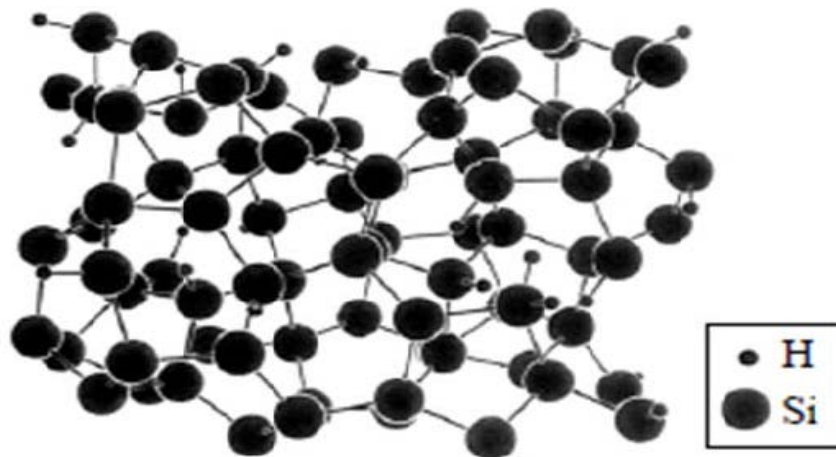


Fig (1-1): Structure of hydrogenated amorphous silicon [9].

1.2.1 Optical Properties

The minimum photon energy that is needed to excite an electron into the conduction band is associated with the bandgap of a material. When electron-hole pairs undergo recombination, photons are generated with energies that correspond to the magnitude of the band gap. A phonon is required in the process of absorption or emission in the case of an indirect bandgap. There must be a direct bandgap in applications of optical devices [12].

1.2.1.1 Direct and Indirect Optical Transition

The band gap of a semiconductor is always one of two types, a direct band gap or an indirect band gap. The minimal - energy state in the conduction band and the maximal - energy state, in the valence band, is each characterized by a certain crystal momentum (k Vector) in the Brillouin Zone. If the k vectors are the same ($\Delta k = 0$), it is called a "direct band gap" and if they are different ($\Delta k \neq 0$), it is called an "indirect band gap"[12]. The band gap is called "direct" if the momentum of electrons and holes is the same in the conduction band and the valence band, which means, an electron can directly emit a photon. While, in an "indirect" gap, this means that the bottom of the conduction band occurs in a different region of k - space than the top in the valence band [13]. According to that, such transitions in amorphous silicon must involve some mechanisms for conserving momentum [14], as shown in Fig (1-2-a, b).

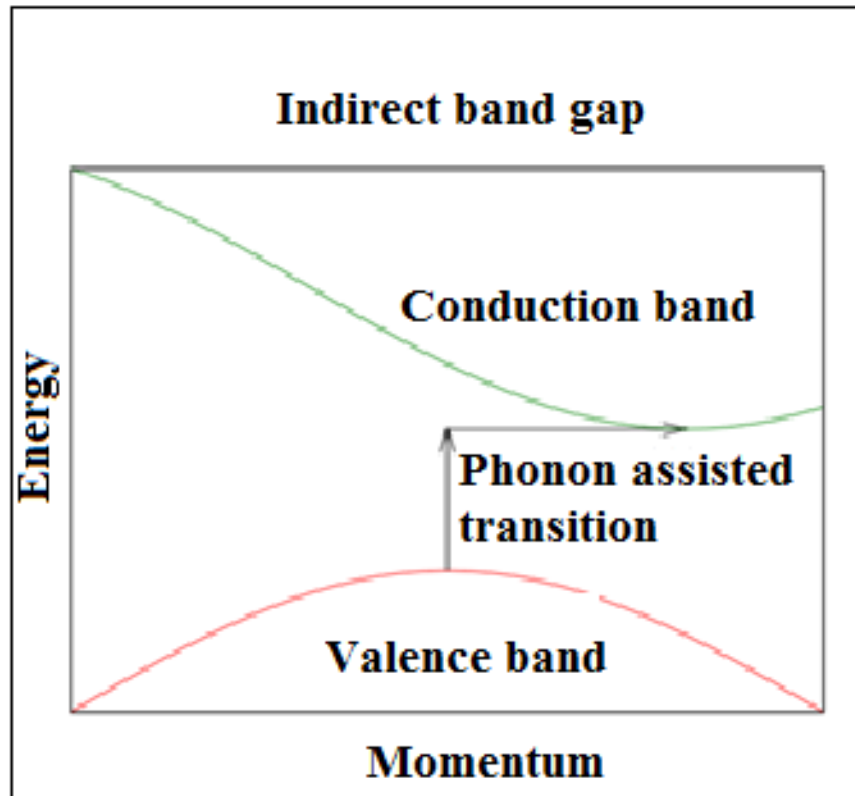
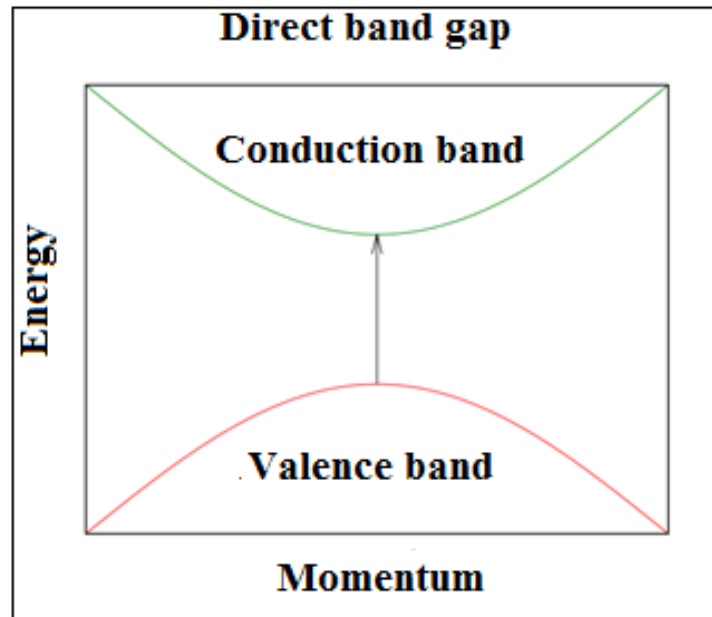


Fig. (1-2-a) Energy vs. crystal momentum for a semiconductor with an indirect band gap, showing that an electron cannot shift from the lowest-energy state in the conduction band (green) to the highest-energy state in the valence band (red) without a change in momentum. Here, almost all of the energy comes from a photon (vertical arrow), while almost all of the momentum comes from a phonon (horizontal arrow) [14].



Fig(1_2_b) Energy vs. crystal momentum for a semiconductor with a direct band gap, showing that an electron can shift from the lowest-energy state in the conduction band (green) to the highest-energy state in the valence band (red) without a change in crystal momentum. Depicted is a transition in which a photon excites an electron from the valence band to the conduction band [14].

1.2.1. 2 Nano Silicon

As far as Silicon has an indirect band gap, it means that the minimum of the conduction band and the maximum of the valence band have different momentums, so electrons in the conduction band can only annihilate holes in the valence band with the help of phonons assistance. However, the probability of electrons and phonons interacting in silicon is low [14], and so this widely used material is

actually a very inefficient light emitter. Many methods have been developed that can improve the light emitting properties of silicon by what is called quantum – confinement effects. This phenomenon has been found to be particularly effective [15], by very small size of a-Si quantum dot which changes the nature of silicon optical band gap from indirect to direct transition material [16].

1.2.2 Electrical Conduction

1) Extended State Conduction

Conduction via extended states by thermal activation of carriers from E_f to above the mobility edge follows the relation

$$\sigma_{ext} = \sigma_o e^{[(E_c - E_f)/KT]}$$

Where σ_o (pre-exponential factor) is the average conductivity above the mobility edge [17]. The extended state conduction, in general, happens at high temperature (above the 300 K⁰).

2) Band Tail Conduction

The conduction in this region is due to the excited charges in the localized level and hopping at the bands edges and hopping at the energy near E_A , E_B . It follows the relation

$$\sigma = \sigma_1 \exp[-(E_A - E_f + \Delta W_1)/KT]$$

Where W_1 is the hopping activation energy. E_A and E_B represented the extended mobility edges of the mobility gap near conduction and valence edges

respectively. This conduction happens at temperature less than that of extended state conduction [17].

c) Hopping Conduction

A well known process in amorphous semiconductors, in general, at low temperature less than room temperature, say less than 300 K, is associated with hopping process within deep localized states in the middle of the gap ($E_A < E < E_B$) [17]. The following relation gives this process $\sigma = \sigma_2 \exp[-w_2/KT]$, Where w_2 is the hopping energy.

1.3 Generation and Recombination of (e-h) Pair

Recombination of electron-hole pairs is a process by which both carriers, annihilate each other [18]: Electrons occupy – through one or multiple steps – the empty state associated with a hole. Both carriers eventually disappear in the process. The energy difference between the initial and final state of the electron is released in the process. This leads to one possible classification of the recombination processes. In the case of radiative recombination, this energy is emitted in the form of a photon. In the case of non – radiative recombination, it is passed on to one or more phonons [19]. While in the case of Auger's recombination it is given off in the form of kinetic energy to another electron. Another classification scheme considers the individual energy levels and particles involved [18]. These different processes are further illustrated in Fig (1-3).

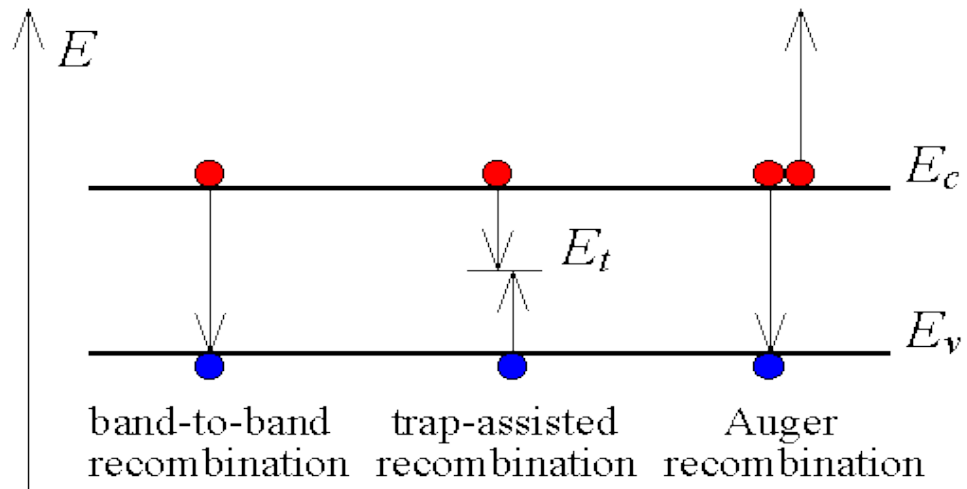


Fig (1-3): Carrier recombination mechanisms in semiconductors [18].

In this work, the radiative recombination process in amorphous silicon is considered. Radiative recombination occurs with transition from the delocalized states of conduction band to the delocalized state of valence band [18], where the electrons are relaxed to the valence band with photons emission [19]. The probability of radiative recombination for an electron is proportional to the number of free holes. Therefore, the rate of this process on the concentration of electrons in the conduction band and holes in the valence band [19, 20]. Also, this process may occur between the delocalized state and the band tail state [21]. Fig (1-4) shows the probabilities of radiative recombination. Each of these recombination mechanisms can be reversed leading to carrier generation rather than recombination. In addition, there are generation mechanisms, generation of carriers by light absorption or by high – energy / particle

beam. Mechanisms are illustrated in Fig. (1-5). And carriers can be generated by illuminating the semiconductor with light. The energy of the incoming photons is used to bring an electron from a lower energy level to a higher energy level. In this case where an electron is removed from the valence band and added to the conduction band, an electron – hole pair is generated [22].

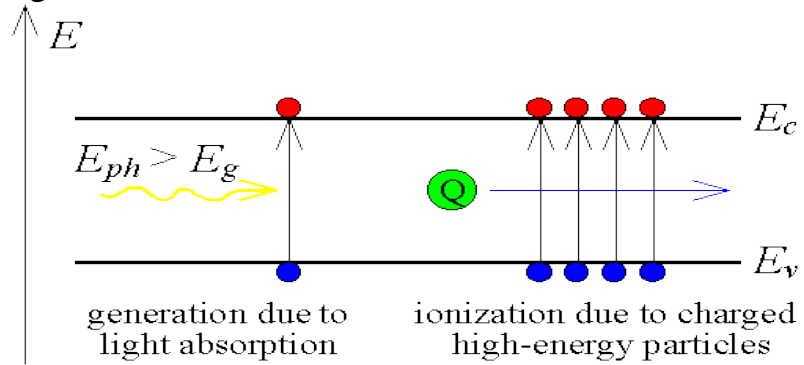


Fig (1-4): Carrier generation due to light absorption ionization due to high-energy particle beams [18].

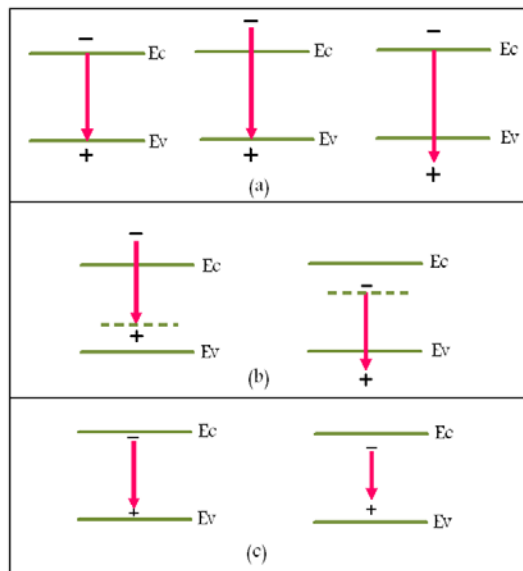


Fig. (1-5): The probabilities of radiative recombination [18]:

- (a) Delocalized to delocalized states;
- (b) Delocalized to localized
- (c) Localized to localized state.

1.4 Semiconductors Nanostructure

The low-dimensional semiconductor structures have broad areas of high research activity [23]. They have promising potential applications in such fields as nonlinear optics, light emitting materials, optoelectronics devices [24], and new applications opened up in optical communications [25]. The strongly related to the realization of such applications, and equally challenging, are the understanding of scaling laws of electronic and optical properties of these materials as the size gradually changes from the bulk semiconductors into molecular systems [26]. However, when these materials are defined as having at least one dimension between 1 to 100 nm they are called nanostructure materials [27-29]. Nanostructures are prepared by new fabrication technologies, where size control, shape control and uniformity can be obtained, by new preparation technologies, with the precision of nanometer scale [30, 31]. The description of these structures by only the nanoscale is very general criterion, which actually includes diverse physical situations [29]; first, each nanostructure material is associated with a specific novel property or a significant improvement in a specific property resulting from the nanoscale structuring. Consequently, the type of nanostructuring used must be based on a spatial dependence of some parameter related to the property under consideration. This parameter could be, for example, the

material density, transport parameters, or dielectric constant. Second, in addition to the nanometer-scale structuring, a larger scale ordering of the unit patterns may be necessary for the existence of the property sought. For example, the particular optical properties of opals require the silica nanospheres to show a long-range order with a coherence length well beyond a micron, for example; the quantum-well superlattice. In other cases, the nanosized building blocks do not need long-range order to provide a specific property, but still require some degree of short-range organization [30]. For instance, an electrical conductivity shows only a critical percolation density for the conducting particles. Finally, some properties of nanostructures materials simply reflect a corresponding intrinsic property of their individual building blocks. This is the case, for instance, in nanoparticle embedded in glass or polymer matrices for optical-filtering applications. In these structures, the physical, magnetic, electrical and optical properties can be altered [30, 32]. Many potential benefits of nanotechnology arise from the fact that engineered nanostructure materials exhibit properties and behavior different from those of the same materials in bulk or macroscopic form [28]. Such structures have received steadily growing interests as result of their small size, peculiar and fascinating properties and applications superior to their bulk counterparts [27]. Taking in account this important note; some nanostructures have no

bulk equivalent, but are made by forming new nanostructures by "building up" from atoms and molecules [28]. The properties of emergence of those materials and their potential used in designing new and more efficient microelectronic devices constitute the most important motivations of the strong ongoing interest in low-dimensional systems [23].

1-4-1 The Classification of Low-Dimensional Structures

Low-dimensional structures are usually classified, according to the number of reduced dimensions, to four types. More precisely, the dimensionality refers to the number of degrees of freedom in the particle momentum. Accordingly, depending on the dimensionality [33, 34], the following classification is made.

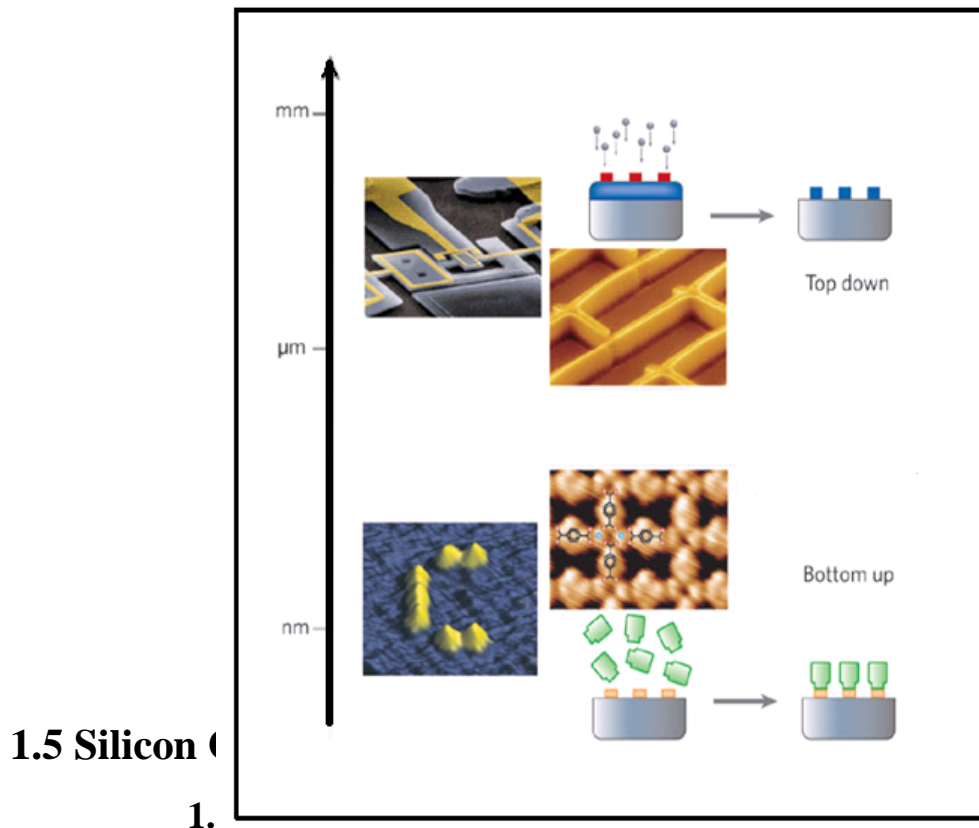
The three-dimensional (3D) structure or bulk structure, no quantization of the particle motion occurs, i.e., the particle is free in the structure of the material. Two-dimensional (2D) structure or quantum well: Quantization of the particle motion occurs in one direction, while the particle is free to move in the other two directions. One-dimensional (1D) structure or quantum wire: Quantization occurs in two directions, leading to free movement along only one direction. Zero-dimensional (0D) structure or quantum dot (sometimes called "quantum box"): Quantization occurs in all three directions.

1-4-2 The Fabrication Technology

Obviously, nanostructures have numerous commercial and technological applications in the areas of electronic, magnetic, optical, and mechanical devices [35]. Therefore, one of the challenges of nanotechnology is the fabrication of nanostructures with controlled size, shape, reproducible and spacing [36], while it may be based on material-specific peculiarities of nanostructures [37]. The impressive in the fabrication of nanostructures has made it possible to reduce the effective devices dimensions from 3-D bulk materials, to 2-D quantum well systems, to 1-D quantum wires, to 0-D quantum dots [38]. By taking that to account; the dimensions of these devices must be smaller than a characteristic length, such as de-Broglie wavelength or Bohr radius [39]. This reason makes nanostructures technology a subject of both fundamental and practical physical interest [40]. Thus, research efforts was devoted to study and develop strategies to reliably create complex systems overall length scales [30]. However, the techniques for creation of nanostructures can be divided into two broad categories[28,30,41]: The first category is the top-down techniques which consist in downscaling the patterning of materials to nanometer size [28], that are involved starting with a bulk or macroscopic materials and obtaining a nanostructure by structural decomposition [41]. This allows

the generation of materials, which are coherently and continuously ordered from macroscopic down to nanoscopic sizes [28]. These techniques, in fact, are used in lithographic [39] and mask techniques [40]. Lithography is considered as the most critical procedure of defining dimensions of structures [39]. The new types of the lithographic systems with higher resolution are desired, for the application in nanostructure, including electron beam direct writing [39, 42]. This offers the great flexibility in design and process and allows creating the extremely fine patterns required by the modern electronic industry for nano-integrated circuits [31, 39]. Beside the electron beam lithography, there are many other types such as X-ray lithography, optical lithography, etc, [37]. The second type of category of nanostructures technology is the bottom-up techniques. These techniques utilized growth and self-assembly [41] to build nanostructures from atomic or molecular precursors [43]. These techniques are started with atoms, ions, or molecules which are defined as " building blocks" [55, 57] and assembled nanoscale clusters or bulk material from them [40]. In this case, structure size can be reached which is not limited by wavelengths and mask sizes [39]. The ability to grow these structures with well- controlled dimensions and compositions has been made possible by rapid advances in modern fabrication techniques such as molecular beam epitaxial (**MBE**), metal-organic chemical vapor deposition

(MOCVD), and their several variants such as chemical beam epitaxy, atomic layer epitaxy, migration enhanced epitaxial, etc..[44]. In general, bottom-up assembled nanoscale electronics could provide unparalleled speed, storage, and size reductions and hold the promise of powering future electronic devices that can outperform existing devices and open up totally new opportunities [43]. It is important to mention that: in nanotechnology, typically difficult to create structures smaller than 50 nm with top- down approaches, while it is often to create structures larger than 50 nm by bottom- up approaches [30]. Fig (1-6) shows the both nanostructure techniques with their scale.



SiQDs have several classifications, all classifications lead to an increase of the band – gap with decreasing crystalline size due to the quantum confinement [32]. These classifications are crystalline silicon quantum dots c – SiQDs, amorphous silicon quantum dots a – SiQDs, and porous silicon p-Si [47]. c-SiQDs receive wide spread interest because of their potential ability to combine electronic and optical functionality in Si-based devices, partially the light emitting devices [53, 54]. But, in the process of searching for more efficient materials of lower dimension, it has been found that the amorphous silicon quantum dots, a-SiQDs, may be convenient material for this purpose [55, 56]. In bulk amorphous silicon two important advantages are compared with crystalline silicon [57, 58]:- firstly, the luminescence efficiency in a-Si is higher than in c-Si due to its structural disorder. Secondly, the band gap energy of a-Si (1.6 eV) is larger than that of c-Si (1.1 eV). Therefore, a-Si is believed to be a good candidate for short wavelength light emitters [59]. Porous silicon is made by silicon crystallites having nanometric dimensions [32]. Porous silicon is simple and cheap, it is very easy to have a high density of emitting center.

1.5.2 Confinement in nano-silicon

The confinement of a carrier means a strong spatial localization of the same carrier [49]. It is considered as a key feature in these new materials [44], it may occur in one dimension, two dimensions and zero dimension [28, 2]. In a 2-D structure, there are only two directions for the movement; the third direction determines the confinement direction. In a 1-D structure, the free movement is possible in only one of the three directions, while in the two remaining directions confinement occurs. In a 0-D structures, there is a total confinement in each direction and the considered particle cannot move freely any more. On the other hand, there is no confinement of the carrier in bulk material because the carrier is free to move in every direction [28, 32].

1.6 Light Emitting Diode

1.6.1 Heterostructure LED

The basic structure of light emitting diode is a p-n junction. Under forward bias, minority carriers are injected from both sides of the junction. At the vicinity of the junction, there is an excess of carriers over their equilibrium values ($pn > n_i^2$), and recombination will take place. This condition is shown in fig (1-7-a). However, if a heterojunction is utilized in the design, the efficiency can be much improved. Fig. (1-7) shows that the central material where light is produced is bound by layers with a higher

energy gap. If the heterojunctions are of Type-I (straddling heterojunction), excess carriers of both types are injected and confined at the same space. As can be seen in fig. (1-7b). The number of excess carriers can be significantly increased the radiative recombination lifetime is shortened, leading to more-efficient radiative recombination. In this band structure, the central layer is undoped bound by layers of opposite types. This double-heterojunction design yields the highest efficiency and is the preferred approach. Furthermore, if the central active layer is reduced to the range of 10 nm or smaller, a quantum well is formed. In this case, the 2-dimensional carrier densities become relevant and have to be calculated based on quantum mechanics. The effective 3-dimensional Carrier densities (per unit volume), however, is given by the 2-D values divided by the quantum-layer width. This phenomenon pushes the carrier densities to higher levels and can result in higher efficiency. Another advantage of a growth, since a thin strained layer can accommodate higher level of lattice mismatch [2].

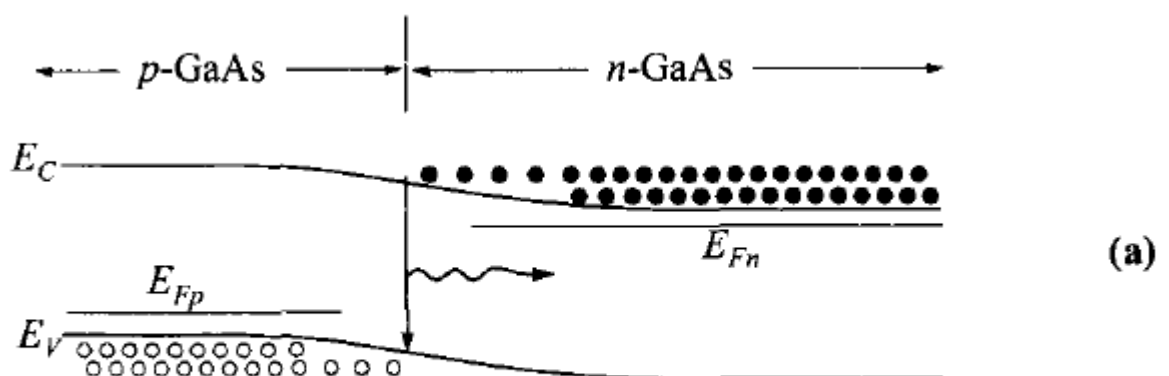


Fig (1-7): (a) Under forward bias of a p-n junction, electrons injected from n-side recombine with holes injected from p-side. (b) Higher carrier densities and improved carrier confinement in a double heterojunction [3].

This double-heterojunction design yields the highest efficiency and is the preferred approach. Furthermore, if the central active layer is reduced to the range of 10 nm or smaller, a quantum well is formed. In this case, the 2-dimensional carrier densities become relevant and have to be calculated based on quantum mechanics. The effective 3-dimensional Carrier densities (per unit volume), however, is given by the 2-D values divided by the quantum-layer width. This phenomenon pushes the carrier densities to higher

levels and can result in higher efficiency. Another advantage of a thin active layer comes about in epitaxial growth, since a thin strained layer can accommodate higher level of lattice mismatch [2].

1.6.2 Nanostructure LED

The nano structure emits higher intensity of light by varying its size. The diameter of one dimension between 1 to 100 nm, and the dots size of zero dimension confinement between 1 to 10 nm. For nanostructure LED must be controlled by its size and shape [30, 31]. In strong quantum confinement structure, like nano wires and nano dots, it can contribute to LED efficiency by pushing holes and electrons to be closer together to enhance the radiative recombination process. Bringing the electrons and holes closer together in the nano structure will increase the probability that they will recombine and emit light. By decreasing the dot size, the band gap can be raised from 2 to 3 eV, and consequently a blue shift in energy of the emitted light.

1.7 Literature Survey

In 1940, after the development of the p-n junction, LED structures were changed from point contacts to p-n junctions. During 1964-1965, significant advancement was made on indirect – band gap materials by introducing isoelectronic impurities [60, 61]. In the early 1970, Pankove published a

metal [In surface contact] – insulator [Zn doped n-GaN] – semiconductor (p-GaN) diode as the first current – injected GaN green and blue (475 nm) light emitter [4]. In 1990, Shuji Nakamura demonstrated the first high – brightness blue LED based on GaInN. In 2000, development of heterostructures [Nobel Prize to Z.I. Alferov and H. Kroemer], and later quantum wells, allowing for a better confinement of the carriers while reducing the losses [61]. In 2005, researchers at Vanderbilt University found that CdSe quantum dots emit light when excited by UV light. In 2006, Nakamura was awarded Millennium Technology Prize for his invention of blue, green and white light – emitting diodes (LEDs) and the blue laser diode. In 2013 he features news research in UV light for food storage, printable quantum dots LEDs, and smart phone disease detection. In 21 April 2013 the high – efficiency quantum – dot light – emitting devices with enhanced charge injection was published [62]. Finally, on October 7, 2014, the Nobel Prize in physics was awarded to Isamu Akasaki, Hiroshi Amano and Shuji Nakamura for the mention of efficient blue light – emitting diodes, which has enabled bright and energy – efficient white light sources or less formally [63].

1.8 The Aim of Present Work

The aim of this work is to investigate the internal quantum efficiency of light emitting diode structure from a-

SiQDs by changing the quantum dot size, injection current and carrier lifetime. By controlling on such parameters, one might obtain physical ideas to achieve the main points, which should be of very important for application in Nano laser devices of amorphous silicon quantum dots.

Chapter

Two

**Theory
And
Calculations**

2.1 Introduction

It is become very well known that the a-Si QDs structure is considered a suitable and a promising candidate for optoelectronics applications. The a-Si QD has many specific possible origins: First, size effects, which results the confinement of a physical entity inside an element [29]. An example is the confinement of electron wave functions inside a region of size smaller than the characteristics length [87]. This class of effects may give birth to completely new properties for a-Si material compared with that of its bulk structure [29, 88]. Second: boundary effects, which are a consequence of the significant volume fraction of matter located near surface, or domain wall [29]. Third; surface effects, which heavily influence the thermodynamics properties [89]. The quantum dot structures are, generally, designed to use quantum confinement to shift the silicon luminescence into the visible region [90]. Therefore the quantum confinement effect is considered as one of the luminescent mechanisms; but it is differing from the other mechanisms by the controlling of the size that could be tunable [58, 94]. In this chapter, the most important assumptions and mathematical equations for a-Si QD LEDs model photoluminescence have been investigated. It starts by nano LED doped structure. Quantum dots LED confinement and properties. Electrical properties of LED, and a-Si QDs as light emitters. Then density of states for all type of quantum confinement. Delta function define and properties. Finally, the

calculations of this model by (I-V) characteristics and fitting for (I-V) curve.

2.2 Nano LED

2.2.1 Structure of Doped Nano LED

Nano structure is any structure with one or more dimensions measuring in the nanometer 10^{-9} m range. Nanostructure of LED in zero-dimension, in this structure the dot size is controlled on quantum efficiency. When the dot size decreases the internal quantum efficiency increases. Dot size from 1.8 nm to 5 nm and the bandgap of energy of bulk silicon is 1.56(eV) is used in these calculation. To obtain on internal quantum efficiency for light emission from nanostructure LED doping layer on a-Si QD LED (opaque doping) [64-71]. So in this work, the structure of Ni/Au contact on silicon nitride containing a-Si QDs is adopted in an attempt to improve current injection and light internal efficiency of a-Si QD LEDs [72, 73]. 38 nm silicon films containing a-Si QDs were grown by plasma enhanced chemical vapor deposition (PECVD) [72-73], in which nitrogen-diluted 5% SiH_4 and NH_3 were used as the sources of reactants. A slowly doped p-type Si wafer (100) with a hole concentration of about 10^{15} cm^{-3} was employed as a substrate. The Ni (9 nm)/ Au (21 nm) contact deposited on the silicon nitride films was annealed in an air ambient for 80 sec. Figure (2-1) shows the current-voltage (I-V) characteristics of a-Si QD LEDs with Ni/Au contact annealed at 400 °C in air. The forward voltage 8.5

V for the annealed Ni/Au contact, at input current of 20 mA. It should be noted that the forward voltage of LED with an annealed Ni/Au contact was drastically decreased by 5 V. The series resistance of the LED with annealed Ni/Au contact was also decreased. This is attributed to the decrease in resistance $2.46 \Omega/\text{sq}$ for the annealed Ni/Au contact [79]. The energy gap (E) for three-dimensionally confined a-Si QD can be expressed as $E \text{ (eV)} = E_{\text{bulk}} + c/d^2$ based on an effective mass theory, where E_{bulk} represent the bulk a-Si band gap, d the dot size in nm, and c the confinement parameter. The data in fig (2-2) are best fitted by the equation $E \text{ (eV)} = 1.56 + 2.4/d^2$ [79]. The fitted fig (2-2), the emission color could be changed by controlling the dot size. Fig (2-3) shows the structure of a-Si QD LED which has been adopted in this work.

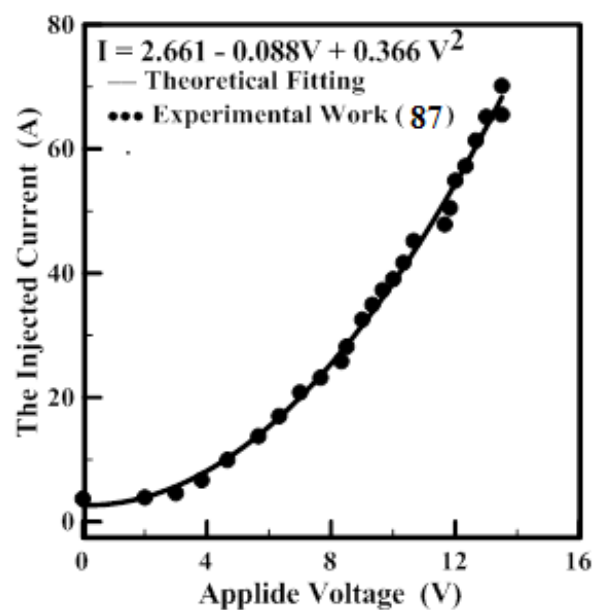


Fig. (2-1): shows the current-voltage (I-V) characteristics of a- Si QD LED Ni/Au contact annealed at 400 °C in air [79].

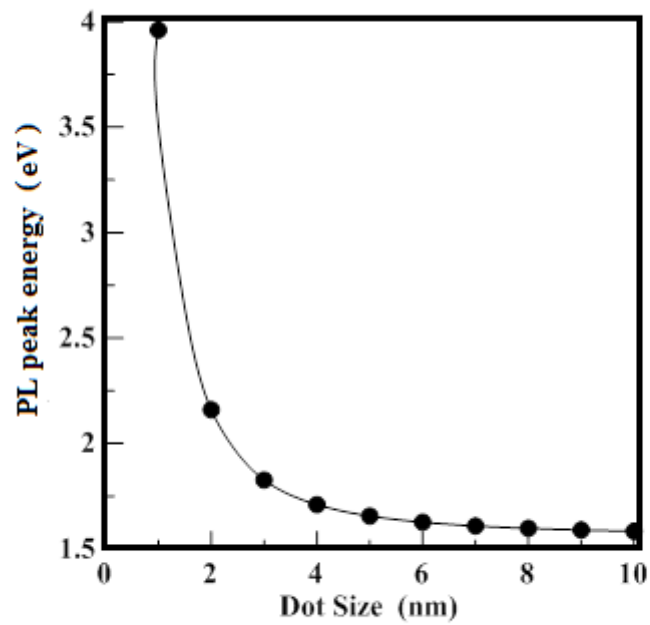


Fig. (2-2): PL peak energy of a-Si DQs as a function of dot size a-Si QDs [74].

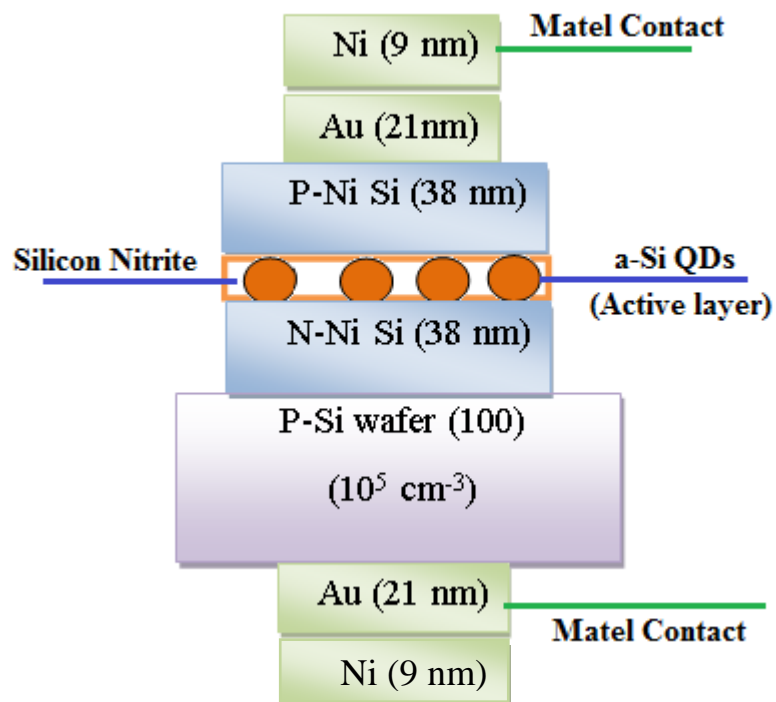


Fig. (2-3): The structure of a-Si QD LEDs, [80].

2.2.2 QDs LED

Quantum dots based LEDs are characterized by pure and saturated emission colors with narrow bandwidth. Their emission wavelength is easily tuned by changing the size of the quantum dots. Moreover, QD-LED offer high color purity and durability combined with the efficiency, flexibility, and low processing cost of organic light – emitting devices OLEDs. Quantum dot LEDs which often contain both organic and inorganic materials each have their own unique advantages, different colors for OLEDs are achieved by different materials, involving different degradation rates and lifetime for each one [81]. This means that display color of these devices generally changes with time. However, in QDLED all of the three primary colors can be obtained with the same composition changing the particle size. Due to the same composition and thus, similar lifetime, the display color variation in QD based devices could be less pronounced. The emission spectra for QD LEDs can reach the IR range, while is rather difficult to overcome the 650 nm peak emission of OLED. It demonstrates the possibility to achieve a really wide range of different emission wavelengths [82]. Atypical QDs LED consist of three layers: one inner layer of quantum dots, one outer layer that transport electrons, and outer layer that transport hole. When an electric field is applied to the outer layers, the electrons and holes move into the quantum dot layer, where they are captured by quantum dots and recombine. The recombination of one electron and hole inside a quantum dot results in emission of the photon, a QD

layer is sandwiched between electron and hole transporting material [82]. An applied electric field causes electron and hole to move into the QD layer where they recombine forming and emitting photons. As a research explained in this letter, a key requirement for achieving QDs LED with high internal quantum efficiency, that one by using 38 nm silicon nitride film containing a-Si QDs were grown by plasma enhanced chemical vapor deposition [72, 73]. Different dot size (1.8, 2, 2.3, 2.7, 3, 3.3, and 3.6) nm was adopted [74], each dot size having different efficiency and wavelength. Green, blue, violet, and white photoluminescence were observed from the a-Si QD structures by controlling the dot size. The turn-on voltage was less than 5 V.

2.2.3 Electrical Properties of LED

A light emitting diode (LED) is essentially a pn-junction diode typically made from a direct bandgap semiconductor, in which the electron–hole pair recombination results in the emission of a photon. When dissimilar doped materials are placed in contact with each other, the flow of current in the region of the junction is different than is in either of the two materials alone. Current will readily flow in one direction across the junction, but not in the other, constituting the basic diode configuration. This behavior can be understood in terms of the movement of electrons and holes in the two material types and across the junction [4].

2.3 Amorphous Silicon Quantum Dots as Light Emitter

Silicon is a dominant material in microelectronics technology, but because of its indirect band structure, it has not been possible to use amorphous Si as light emitting devices [45-47]. The recent advancement in silicon technology has led to the fabrication of Zero-dimensional structure, which is called silicon nano crystals or silicon nanoparticle [48]. The exceedingly small region of space is suggested to be named "dot" [49]. Therefore, these structures can be called silicon quantum dots, SiQDs systems [50, 51]. The realization of SiQDs system has opened amazingly new area of physical research and technology that deal with atomic scales. Since the active SiQDs have dimensions that are below ten nanometer [25, 48], the properties of this material completely change for this range of size [32]. Thus, SiQDs systems are considered as potential blocks for future nanoelectronics and nanophotonics [53].

2.4 The density of States

One of the major effects of the confinement is on the shaping of the density of states [8], where It is considered as an important distinction between the low-dimensional systems. The modification of the density of states depends on the degree of confinement [8, 37, 46]. The main idea of this phenomena is that energy states in nanostructures are very different from those in bulk materials due to the quantum size effects on electrons

[62], where the size of these states are restricted to the order of an electron wave function [63]. In the case of a bulk material, the density of states increases with the energy of the particle following a parabolic law [47, 64], where the density of states is proportional to $(E - E^0)^{1/2}$, where E^0 is the energy of the bottom of the band [46,47] as shown in fig. (2-4a). A free 3-D motion in these materials yields a band by three wave vectors K_x, K_y, K_z [46]. The density of states for bulk material can be expressed as [8, 60]:

$$N(E) = \frac{1}{2N^2} \left(\frac{2me^*}{\hbar^2} \right)^{1/2} (E - E^0)^{1/2}$$

Confinement into a 2-D well splits the band into sub bands and leaves only two continuously varying wave vectors K_x, K_y in each sub band [46]. The density of states for each sub band is constant above the energy E_n of the bottom state [46, 64]. Therefore, the overall density of states is discontinuous as shown in fig. (2-4b). In other words, the 2-D density of states is constant and does not depend on energy as shown in this expression [60]:

$$N(E) = \frac{2me^*}{\hbar^2}$$

Confinement in one additional dimension splits each 2-D sub band further into a set of 1-D sub band. Each 1-D is characterized by only one continuously varying wave vector K_x . The density of states corresponding to the sub band n_1, n_2 has a variation of the form $(E - E_{n_1, n_2}^0)^{-1/2}$, with divergence at the bottom of the sub band E_{n_1, n_2}^0 . The density of states of quantum

wire, thus, has a more one pronounced structure than does a 2-D well, with a large number of sub bands, each starting as a peak. 1-D density of states, as indicates in fig. (2-4c) is obtained by [8,

$$60]: \quad N(E) = \frac{1}{\pi\hbar} \sqrt{\frac{me^*}{2}} (E - E_{n_1, n_2}^0)^{-\frac{1}{2}}$$

Finally, confinement in all dimensions creates a completely discrete, atom-like set of states [46]. The density of states of a quantum dot, thus, consists of a series of even sharper spikes, as indicates in fig. (2-4d) which corresponds to a series of confined quantum levels for the electrons in the box [64]. Therefore, the density of states is described by a δ -function [8, 60]:

$$N(E) = 2\delta(E - E_{N_1, N_2, N_3}^0)$$

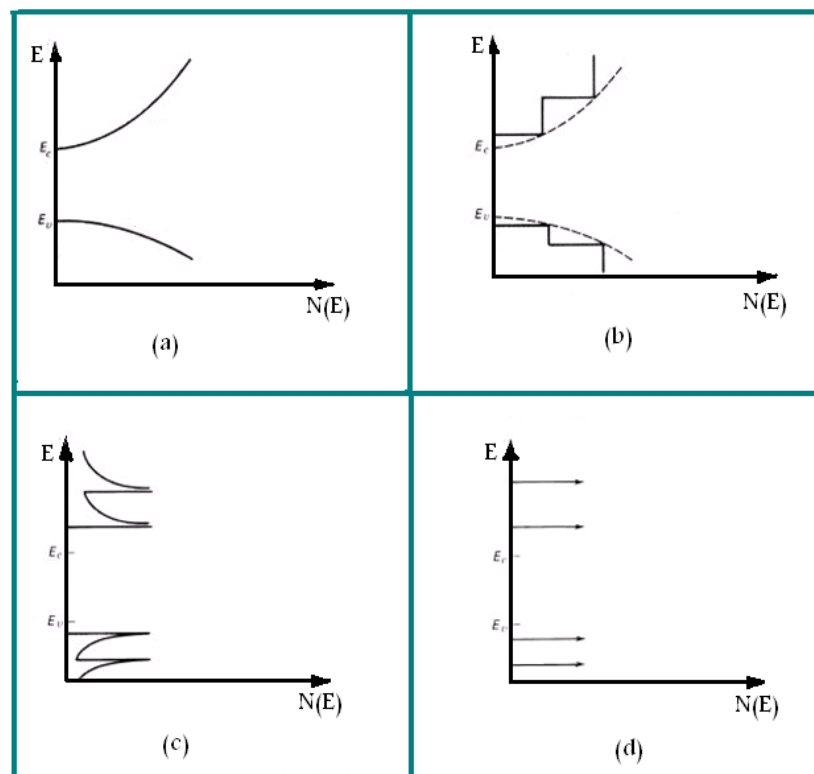


Fig. (2-4): The Density of states for (a) bulk material (b) 2-D structure (c) 1-D structure (d) 0-D structure [53].

2.5 Delta Function

The delta function is a generalized function that can be defined as the limit of the class of delta sequences. The delta function is sometimes called “Dirac’s Delta Function” or the “impulse symbol” [83]. It is implemented in mathematics as “Dirac Delta”. Dirac delta function is defined by the following property:

$$\delta(t) = \begin{cases} 0 & t \neq 0 \\ \infty & t = 0 \end{cases}$$

With $\int_{t_1}^{t_2} \delta(t) dt = 1$, the important property of the delta function is the following relation $\int f(t) \delta(t) dt = f(0)$ for any function $f(t)$. First of all, $\delta(t)$ vanishes everywhere except $t = 0$. Therefore, it does not matter what values the function $f(t)$ takes except at $t = 0$. Then $f(t) \delta(t) = f(0) \delta(t)$. Then $f(0)$ can be pulled outside the integral because it does not depend on t , and are can be obtained [84]:

$$\int f(t) \delta(t - t_0) dt = f(t_0) \quad (2-1)$$

Mathematically the delta function is not a function, because it is too singular. Instead, it is said to be a “distribution”. It is a generalized idea of function, but can be used only inside integrals. In fact, $\int \delta(t) dt$ can be regarded as an “operator” which pulls the value of a function at zero. But as long as it is understood that the delta function is eventually integrated, it can be used as if it is a function.

2.6 LED Efficiency

2.6.1 Internal Quantum Efficiency

The internal quantum efficiency η_{int} gauges what fractions of e-h recombination in the forward biased pn-junction are radiative and therefore lead to photon emission. Nonradiative transitions are those in which e-h recombine through a recombination center such a crystal defect or an impurity and emit phonons [4]. By definition,

$$\eta_{int} = \frac{\text{rate of radiative recombination}}{\text{total rate of recombination}} \quad (2-2)$$

$$\tau_r = \frac{\frac{1}{T_r}}{\frac{1}{T_r} + \frac{1}{T_{nr}}} \quad (2-3)$$

Where τ_r is the mean lifetime of a minority carrier before the radiative recombination and τ_{nr} the mean lifetime before they recombine via a nonradiative recombination center. The total rate of recombination whereas the number of photons emitted per second Φ_{ph} is determined by the rate of radiative recombination [4].

$$\eta_{int} = \frac{\text{photons emitted per second}}{\text{Electrons injected per second}} \quad (2-4)$$

$$= \frac{\Phi_{ph}}{I/e} \quad (2-5)$$

For parabolic electron-hole bands, the LED spontaneous emission rate r_{sp} can be written as [85]:

$$r_{sp} = P_{em} N_j(E) e^{E/kT} \quad (2-6)$$

Where P_{em} is the emission probability, which is the inverse of recombination lifetime τ_r ; Boltzmann distribution function; and $N_j(E)$ is the joint density of state in a zero-dimension system, Equ (2-7):

$$N_j(QD) = 2\delta(E - E_{N1, N2, N3}) \quad (2-7)$$

The spontaneous emission rate can be written as:

$$r_{sp} = 1/\tau_r 2\delta(E - E_{N1, N2, N3}) e^{E/kT} \quad (2-8)$$

The total photon flux Φ_{ph} emitted from the QDs LED is obtained by integrating over r_{sp} :

$$\Phi_{ph} = \frac{2V}{\tau_r} \int_0^\infty \delta(E - E_{N1, N2, N3}) e^{E/kT} dE \quad (2-9)$$

From the properties of delta function in eq. (2-1) the total photon flux Φ_{ph} can be:

$$\Phi_{ph} = \frac{2V e}{\tau_r} e^{E/kT} \quad (2-10)$$

Where E is the energy gap for three-dimensionally confined a-Si QD can be expressed as E (eV) = $E_{bulk} + 2.4/d^2$ [79] based on effective mass theory; v is the volume of the active region. Then compensate equ (2-10) in equ (2-5) we obtain:

$$\eta_{int} = \frac{2V e}{\tau_r I_{inj}} e^{E/kT} \quad (2-11)$$

Where I_{inj} is the injection current, calculated according to the fitting obtain from the paper [79] by using the getdata software. It appears as the following expression:

$I_{inj} = 2.691 - 1.013.V + 0.130. (V^2)$, where V is the applied voltage in volt.

2.6.2 Extraction and external efficiency

The extraction efficiency $\eta_{\text{extraction}}$ is defined as a ratio between photons emitted into the free space and photons emitted by the active region. In a real diode the extraction efficiency never reaches unity. There are many factors having an influence on photon emission into the free space. For example the reabsorption of the photon by the substrate or by the metallic contact. Also the phenomenon of total internal reflection, also referred to as the trapped light phenomenon reduces the ability of the light to escape from the semiconductor [4]. The extraction efficiency is defined by eq. (2-12):

$$\eta_{\text{extraction}} = \frac{\text{photons emitted into free space for second}}{\text{photons emitted from active region per second}} \quad (2-12)$$

$$= \frac{P_{\text{opt}}/h\nu}{P_{\text{opt(int)}}/h\nu} \quad (2-13)$$

Where P_{opt} is the optical power emitted into free space. External quantum efficiency η_{ext} gives the ratio of the number of useful photons to the number of injected charge carriers [4].

$$\eta_{\text{ext}} = \frac{\text{photons emitted into free space per second}}{\text{Electrons injected into LED per second}} \quad (2-14)$$

$$= \frac{P_{\text{opt}}/(h\nu)}{I/e} = \eta_{\text{int}} \eta_{\text{extraction}} \quad (2-15)$$

2.7 The Main Parameters of a-Si

Parameters to calculate internal quantum efficiency. Such as, energy gap of three dimension quantum confined to calculate the energy gap in equation of internal efficiency eq. (2-11). Injections current obtained it from fitting I-V characteristic [79]. Wavelength calculated as a function to internal quantum efficiency from equation $E \text{ (eV)} = 1.24/\lambda \text{ (\AA)}$. Finally, different dot size (1-4) nm to control the a-Si QDs region and emit wavelengths.

2.8 The calculations

2.8.1 Current-Voltage (I-V) Characteristics

The current-voltage (I-V) characteristics of the pn-junction are described by the Shockley equation for ideal diode with cross-sectional area A as followed [86]:

$$I = e A \left(\sqrt{\frac{D_p}{\tau_p}} \frac{n_i^2}{N_D} + \sqrt{\frac{D_n}{\tau_n}} \frac{n_i^2}{N_A} \right) (e^{eV/kT} - 1) \quad (2-16)$$

Where $D_{n,p}$ and $\tau_{n,p}$ are the electron and hole diffusion constant and minority carrier lifetime, respectively. Under typical forward bias conditions, the diode voltage $V \gg kT/e$ and thus $[\exp(eV/kT) - 1] \approx \exp(eV/kT)$. Using equ. (2-17)

$$V_D = kT/e \ln N_A N_D/n_i^2 \quad (2-17)$$

Where n_i^2 is the intrinsic carrier concentration of the Semiconductor [4].

$$I = e A \left(\sqrt{\frac{D_p}{\tau_p}} N_A + \sqrt{\frac{D_n}{\tau_n}} N_D \right) e^{e(V - V_D)/kT} \quad (2-18)$$

In this work, the use of Ni/Au contact on silicon nitride containing a-Si QDs was adopted in an attempt to improve current injection and the internal quantum efficiency of a-Si QD LEDs. But it is difficult to inject carriers from the contact layer into a-Si QDs via the insulating layer since the insulating layer such as a silicon nitride or silicon oxide film which contains the a-Si QDs serves as an energy barrier for the quantum confinement of the charge carriers in the a-Si QDs [79]. To inject carriers from contact metals into a-Si QD LEDs, a highly doped polysilicon, indium tin oxide (ITO), semitransparent Al, Ti, and Au thin films have been employed as contact materials. Figure (2-1) shows the current-voltage (I-V) characteristics of a-Si QD LEDs with annealed Ni/Au contact at 400 °C in air. Also, it should be noted that the forward voltage of an LED with annealed Ni/Au contact was dramatically decreased by 5 V [79].

2.8.2 The Fitting for Current-Voltage (I-V) Curve

In this fitting for (I-V) curve, fig (2-1) shows the (I-V) characteristic of a-Si QD LEDs with an annealed Ni/Au contact in Get Data program to get all the data for current and the voltage, using Get Data Graph Digitizer version 2.26.0.20, copyright 2002-2013, S, Fedorov. After getting all the data by Get Data program (software) Graphic program-version 10.1.640 (32 bit), February 18 2013 to obtain fitting for injection current. The fitting for injection current take the following formula:

$$I_{inj} = 2.691 - 1.013 V + 0.130 V^2 \quad (2-20)$$

Where I_{inj} is the injection current in (Amp) and V is the applied voltage in volt (V). All the calculations have used MathCad Software Version 15.

Chapter Three

**Results,
Discussions
And Conclusions**

3.1 Introduction

Light emission from a-SiQDs structure is a research topic and current interest for applications in silicon-based optoelectronic device [95]. In this work, the light emission in a-SiQDs with size of (1- 4) nm is studied [94]. These sizes can be classified into four regions: the first region that is bulk-like behavior, in the range ($d \geq 3.6$ nm). The second region includes the large dot size which has the range between ($3.6 > d \geq 2.7$ nm). While the third region takes the range ($2.7 > d \geq 2$ nm). Finally, the fourth region is small-dot size that has ($d \leq 1.8$) nm. Each range of these regions has a particular behavior which differs from another range. In this chapter, it will be shown the results of the calculations, internal quantum efficiency as a function of wavelength and injection current. Then, the effect of quantum dot size in internal quantum efficiency and the discussion of results. Finally, the conclusions and suggestions for future work .

3.2 Internal Quantum Efficiency as a Function of Wavelength

3.2.1 The Effect of Recombination Lifetime

Fig.(3-1) and (3-2) show the internal quantum efficiency η_{int} as a function of the wavelength for different values of radiative recombination lifetime τ_r (a) at $\tau_r = 11 \times 10^{-6}$ sec and (b) at $\tau_r = 40$ nsec, at constant temperature. In Fig.(3-1), it is found that, the internal quantum efficiency is higher for τ_r 40 nsec compared with that for $\tau_r = 11 \times 10^{-6}$ sec at room temperature (300 K). The value of internal quantum efficiency η_{int} is also affected by the quantum dot size, and the wavelength which correspond to

the energy gap. Since, the energy gap is a function of quantum size from the equation $E \text{ (eV)} = 1.56 + 2.4/d^2$. The emission color could be changed by controlling the dot size [81], the dot size corresponding to green and blue colors emitted are 2.3 and 1.8 nm respectively [81]. In this spectrum, two peaks are apparent at 3600 and 4000 Å. In Fig (3-2), it is found that, the internal quantum efficiency η_{int} decreased at 200 K comparing with that at 300 K (see Fig. 3-1). As well as, the internal quantum efficiency is higher when the recombination lifetime $\tau_r = 40 \text{ nsec}$. In both radiative recombination lifetime are decreasing at low temperature 200 K. The emission color is from 2800-4000 Å. For example, the dot size corresponding to green and blue colors emitted are 2.3 and 1.8 nm respectively. The tuning of colors emitted and efficient emission can be achieved due to quantum confinement effects [58, 92]. Since quantum confinement effects make silicon a likely candidate for full color display [58].

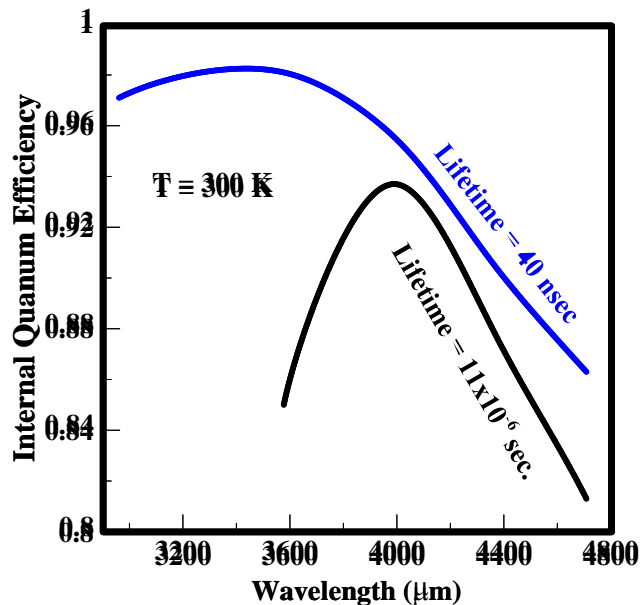


Fig (3-1): The internal quantum efficiency as a function of wavelength at different lifetime.

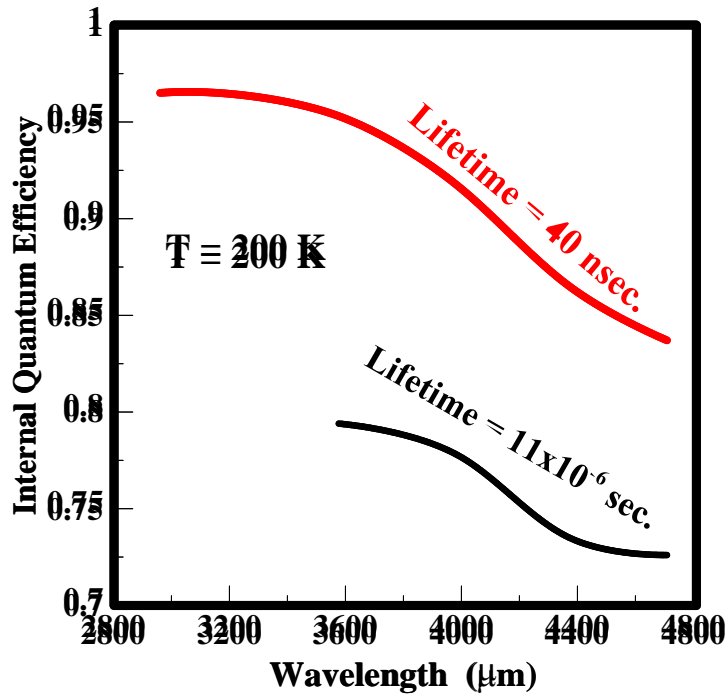


Fig (3-2): The internal quantum efficiency as a function of wavelength with different lifetime.

3.2.2 The Effect of Temperature

Fig. (3-3) and (3-4) show the internal quantum efficiency η_{inj} as a function of wavelength, for two 300 and 200 K and the same recombination lifetime. In Fig. (3-3), it is found that, the internal quantum efficiency η_{inj} is higher when $T=300\text{ K}$ than that at $T= 200\text{ K}$. In this figure the emitted color, that could be changed by controlling the dot size, is tuning from 3200-4800 Å. For example, the dot sizes corresponding to green and blue emission color were 2.3 and 1.8nm, respectively. White luminescence could also be obtained via the deposition of two silicon nitride layers containing the blue-emitting a-Si QDs [74]. In fig. (3-4), it is clear, that the internal quantum

efficiency η_{int} is higher when $T = 300$ K and more than that when $T = 200$ K. However, this result of internal quantum efficiency at $T = 300$ K and the radiative recombination lifetime $\tau_r = 40$ nsec is higher than that at $T = 300$ K and $\tau_r = 11 \times 10^{-6}$ sec, as depicted in Fig. (3-1). Nevertheless, the internal quantum efficiency in both Fig. (3-3) and (3-4) is high when $T = 300$ K. While figure (3-4) shows the emission color could be changed by controlling the dot size, where the tuning of the emission color from 2800-4800 Å. For example, the dot sizes corresponding to green and blue emission color were 2.3 and 1.8 nm, respectively.

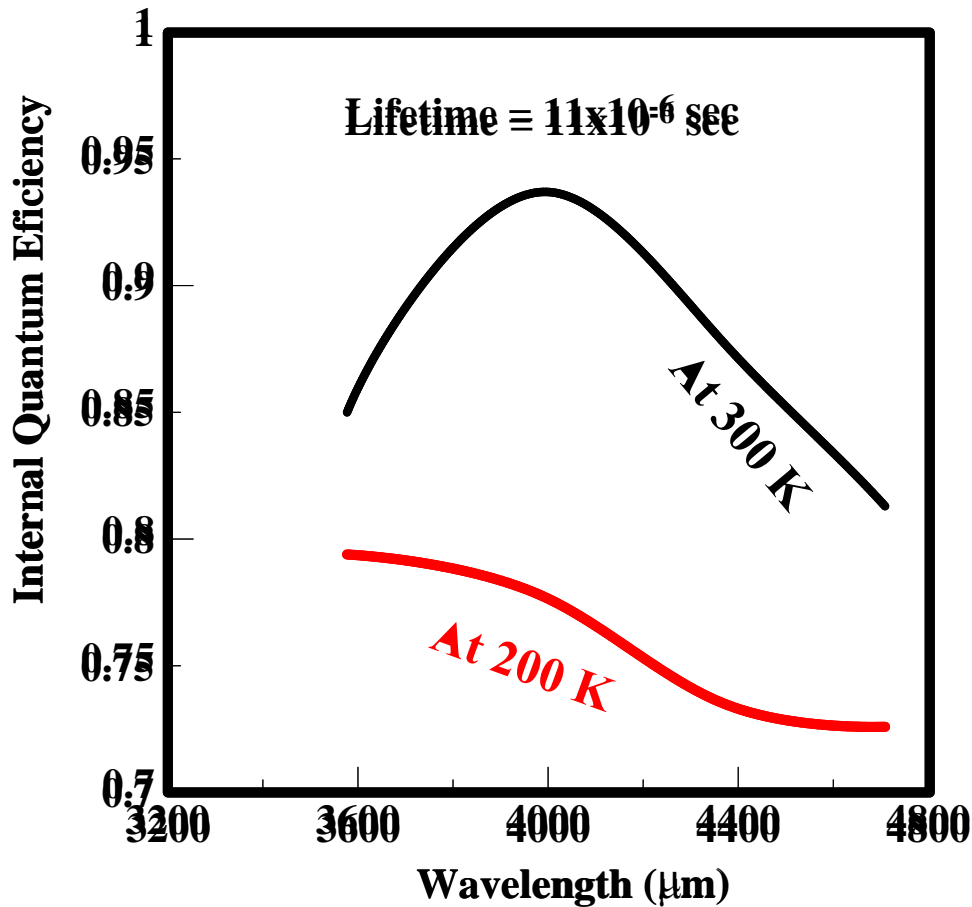


Fig (3-3): The internal quantum efficiency as a function of wavelength at constant recombination lifetime.

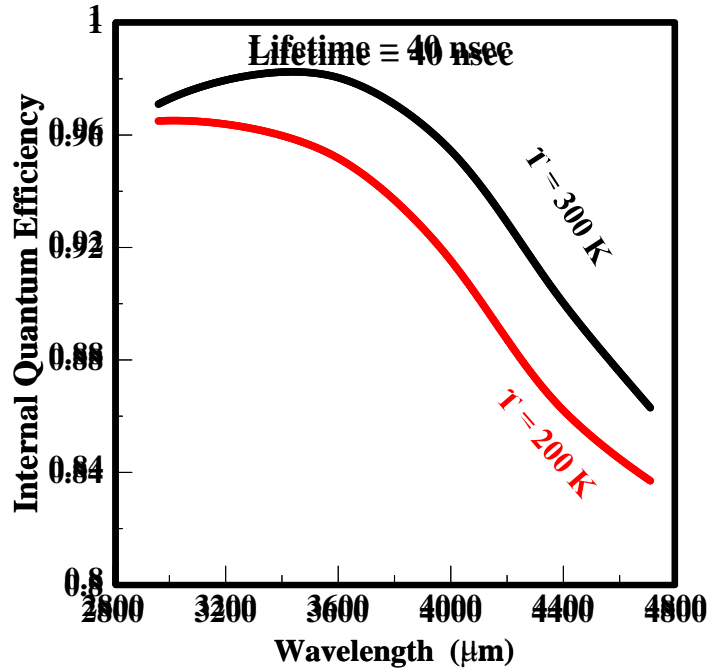


Fig (3-4): The internal quantum efficiency as a function of wavelength at constant recombination lifetime.

3.3 Internal Efficiency As a Function of Injection Current

3.3.1 The Effect of Temperature at dot size 1.8 nm

Figure (3-5) and (3-6), internal quantum efficiency η_{int} as a function of injection current at dot size 1.8 nm and different temperatures. Fig. (3-5) shows the internal quantum efficiency η_{int} as a function of injection current at $\tau_r = 11 \times 10^{-6}$ sec with dot size 1.8 [74]. It is found that, the increasing in internal quantum efficiency η_{int} with decreasing injection current, is higher than in temperature 200 K. In figure (3-6) it is observed that the internal quantum efficiency η_{int} increases with the decrease of injection. As well as, the internal quantum efficiency η_{int} at room temperature is higher than when $T = 200$ k. But the internal quantum efficiency η_{int} in figure (3-6) at $\tau_r = 40$ nsec

is higher than internal quantum efficiency η_{int} at $\tau_r = 11 \times 10^{-6}$ sec and in the same dot sizes 1.8 nm.

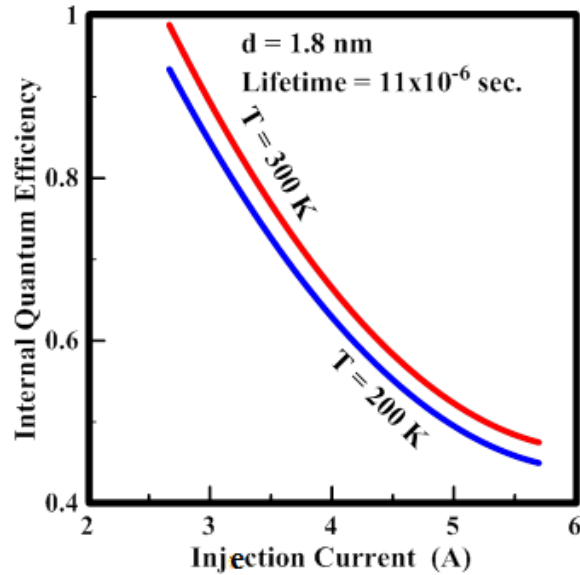


Fig (3-5): The internal quantum efficiency as a function of injection current at different temperatures with recombination lifetime 11×10^{-6} sec.

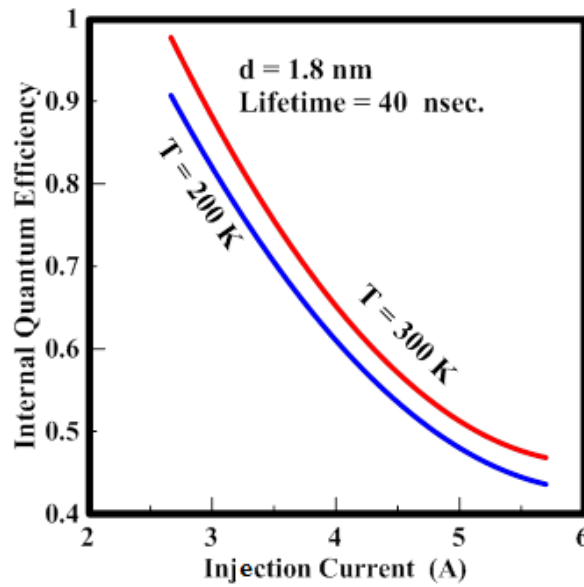


Fig (3-6): The internal quantum efficiency as a function of injection current at different temperatures with recombination lifetime 40 nsec.

3.3.2 The effect of quantum Dot size

Figure (3-7) and (3-8) show the internal quantum efficiency η_{int} as a function of injection current with different temperature and for lifetime 11×10^{-6} sec, at different dot size 1.8, 2.7 and 3.6 nm. It is clear, that the internal quantum efficiency η_{int} increases with decreasing injection current, in both figures. In Figure (3-7), η_{int} is higher at the dot size 1.8 nm than dot size 2.7 and 3.6 nm, at room temperature and lifetime 11×10^{-6} sec. From fig.(3-8), the internal quantum efficiency η_{int} when $T = 200$ K is highest at dot size 1.8 nm. In addition, the observed internal quantum efficiency η_{int} at dot size 2.7 and 3.6 nm is close together. Hence, the η_{int} at room temperature is higher than that when $T = 200$ K at different quantum dot size.

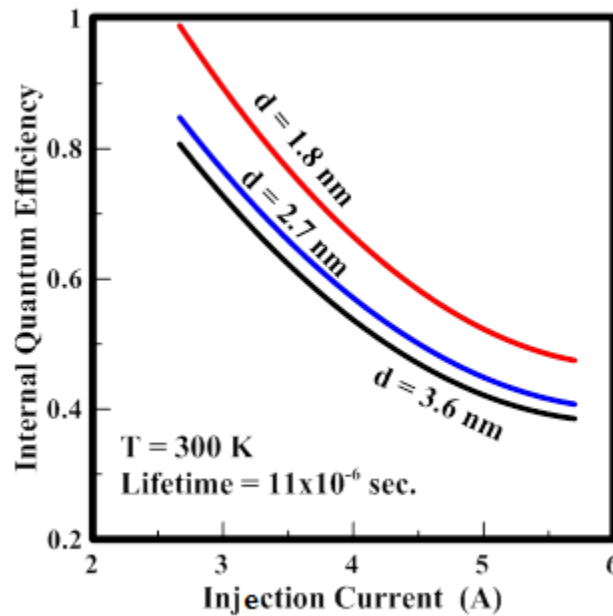


Fig (3-7): The internal quantum efficiency as a function of injection current.

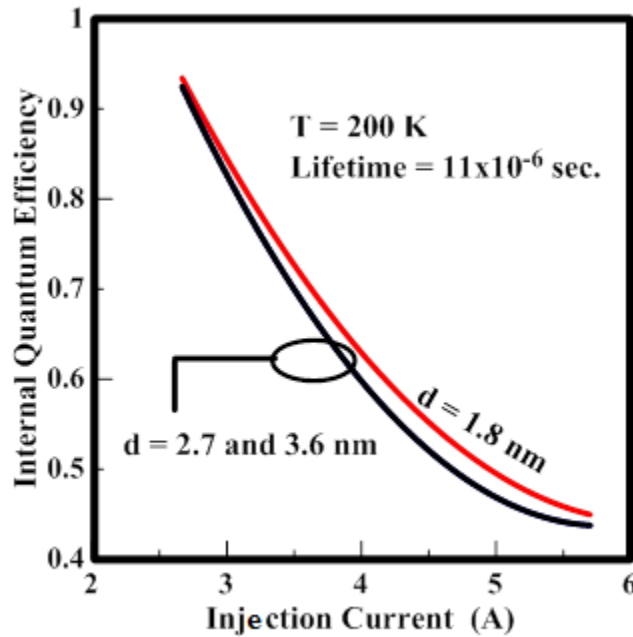


Fig (3-8): The internal quantum efficiency as a function of injection current.

3.3.3 The Effect of Temperature

Figure (3-9) and (3-10) show the internal quantum efficiency η_{int} as a function of injection current at lifetime 40 nsec and different quantum dot size 1.8, 2.7 and 3.6 nm. In both figures the internal quantum efficiency η_{int} increases with the decreasing of injection current. From figure (3-9), the internal quantum efficiency η_{int} is close together at dot size 1.8 and 2.7 nm, and it is higher than when dot size 3.6 nm. This result is at room temperature. From figure (3-10), the internal quantum efficiency η_{int} at dot size 1.8 and 2.7 nm is close to gather but at dot size 1.8 nm the internal

quantum efficiency η_{int} is a bit higher little. As well as, the internal quantum efficiency η_{int} at room temperature is higher than $T= 200$ K.

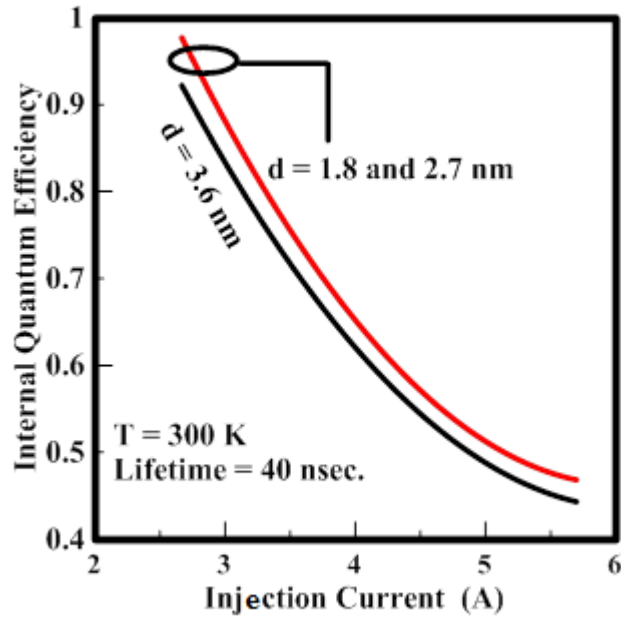


Fig (3-9): The internal quantum efficiency as a function of injection current.

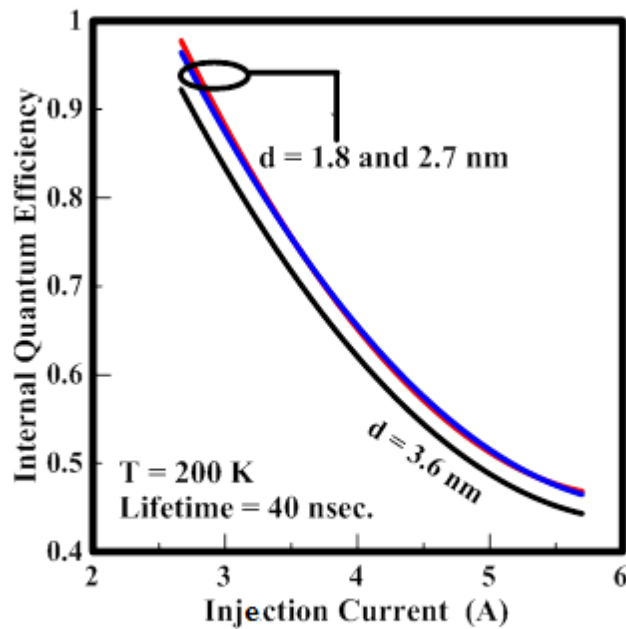


Fig (3-10): The internal quantum efficiency as a function of injection current.

3.3.4 Constant Dot Size and Temperature with Different Lifetime

Figure (3-11) and (3-12) show the internal quantum efficiency η_{int} as a function of injection current, at dot size 1.8 nm [74]. Observed in both figures the η_{int} increase with decreasing injection current. In figure (3-11), the internal quantum efficiency η_{int} at recombination lifetime 11×10^{-6} sec is higher than when $\tau_r = 40$ nsec at room temperature. Also the internal quantum efficiency η_{int} in figure (3-12) is the highest when lifetime 10×10^{-6} sec than $\tau_r = 40$ nsec at temperature 200 K. But the internal quantum efficiency η_{int} in both recombination lifetimes at room temperature is higher than internal quantum efficiency η_{int} at temperature 200 K.

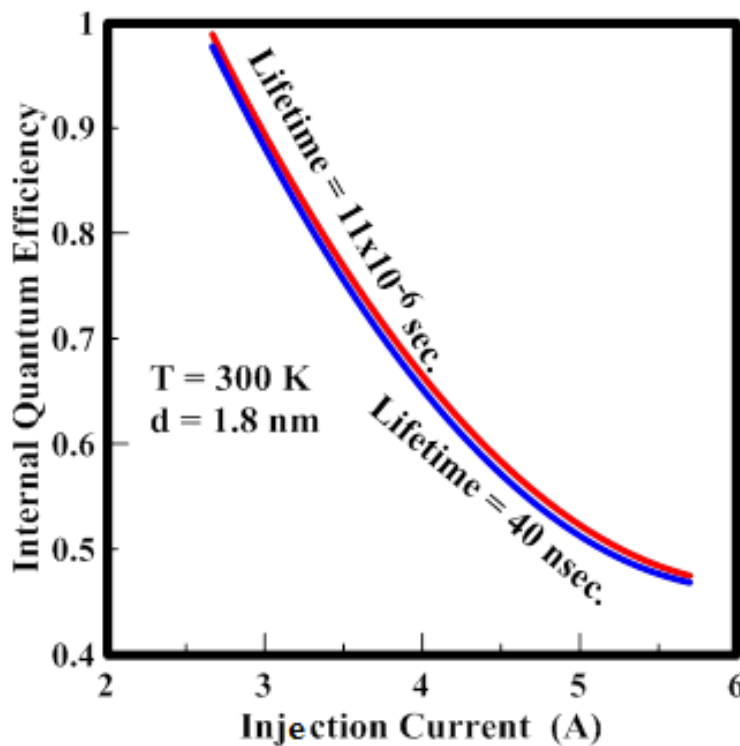


Fig (3-11): The internal quantum efficiency as a function of injection current.

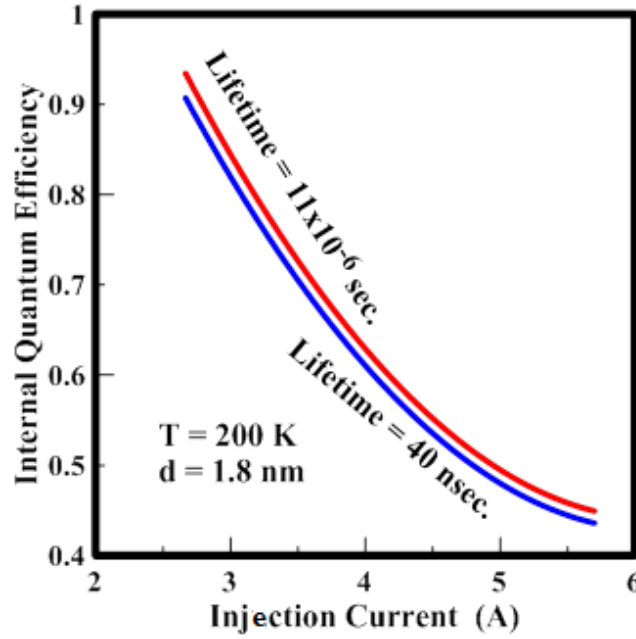


Fig (3-12): The internal quantum efficiency as a function of injection current.

3.4 The Effect of Quantum Dot Size on Internal Quantum Efficiency

Figure (3-13), shows the effect of quantum dot size on the internal quantum efficiency η_{int} for a-Si QDs structure at room temperature and recombination lifetime 11×10^{-6} sec. It is found, that the internal quantum efficiency η_{int} increases when the quantum dot size decreasing. So, whenever a small quantum dot size $d \leq 3.5$ nm is approached a maximum η_{int} and large energy gap is obtained the quantum dot size increases $d \geq 4$

nm minimum internal quantum efficiency η_{int} is obtained and a-Si QDs material have been changed and return to be indirect band gap material [16]. The equation after fitting this figure $Y = -0.0955X + 1.143$, where Y expresses the η_{int} and X is quantum dot size.

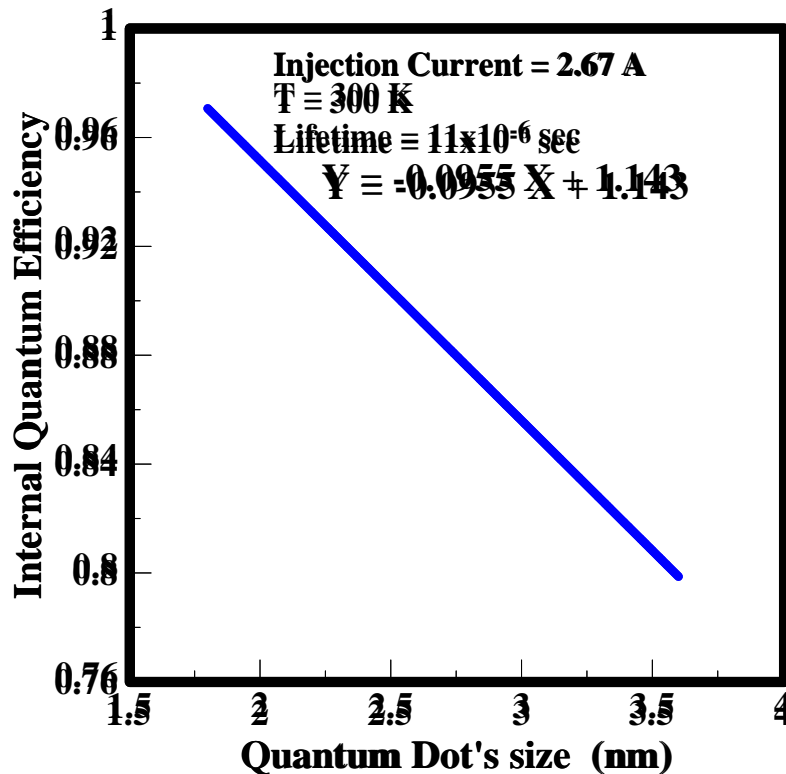


Fig (3-13): The internal quantum efficiency versus quantum Dot size.

3.5 General Discussion

3.5.1 Internal Quantum Efficiency as a Function of Wavelength

The internal quantum efficiency η_{int} of a-Si QDs LED is increasing with temperature, and shows the maximum value of η_{int} at room temperature (300 K). The reason of this result to increase internal quantum efficiency η_{int}

with temperature can be increased in the number of photogenerated carriers with temperature. To explain more about this change in internal quantum efficiency η_{int} with temperature, similar anomalous temperature dependence have been reported for other silicon-based structure [93]. It is observed that similar phenomenon in bulk a-Si:H, which was explained by Auger effect due to nonradiative recombination from the different excitation power dependent PL experiments [93]. Although temperature dependent PL experiments were carried out with different excitation power for our a-Si QDs sample, no difference of the temperature dependence was observed, in contrast to the case of the bulk a-Si:H. However, the internal quantum efficiency η_{int} of a-Si QDs sample increases with temperature and recombination lifetime decrease. The decrease in internal quantum efficiency η_{int} with the increase in temperature and internal quantum efficiency η_{int} caused by the emission probability, it is mentioned in section (2.6.1). The emission probability of photoluminescence in LED is the inverse of recombination lifetime. Therefore, whenever decrease in τ_r the probability of carrier radiative recombination process increases and hence increasing in the number of emitted photons with an increase in internal quantum efficiency η_{int} .

3.5.2 Internal Quantum Efficiency as a Function of Injection Current

The amorphous silicon QDs LED is operated normally under forward-bias condition. The p- (Ni Si 38 nm) and n- (Ni Si 38 nm) layers act as the injectors of holes and electrons, respectively, into the luminescent a-Si QD region. In this kind of band structure, there are two possible processes for

carrier injection into the a-Si QDs. If carriers have a higher thermal energy than the barrier height, they can flow over the barriers. This process is called as “thermionic emission.” This process would play only a minor role since the barrier heights at the p-a-Si and n-a-Si interfaces are much larger than the thermal energy of carriers at room temperature and consequently at 200K another process considered here is field-tunneling through the barriers under high electric field. In this case, the field-tunneling process will be considered as dominate injection current that flows in the a-Si QDs junction. The EL intensity is essentially proportional to the rate of the radiative recombination of electrons and holes. The rate of the radiative recombination is in turn determined by the product of excess electron and hole densities at the initial and final states of the radiative transitions [96]. Therefore, the discussion of all the results of internal quantum efficiency as a function of injection current need somehow more information, which will be considered in the future. But, the main point is how such material, which has been considered as indirect optical energy gap, could make a high radiative recombination transition probability? The answer for this point, hides behind the idea of quantum confinement. The dynamic of quantum confinement for *a-SiQDs* model is characterized by the shifting of energy levels for both conduction and valence bands. This shifting is proportional to the dot size, since the carriers are confined in three-dimensions, which is the case of quantum dots. This leads to the overlap of the envelope wave functions, which is more than in the other nanostructures. However, the shifting of energy levels becomes more when the dot size decreases. This can be explained as: - As the dot size decreases the effective mass of electron (hole) decreases (increases),

therefore; the energy levels are shifted to higher (lower) magnitude of conduction (valence) band, which results from the assumption of $\left(\frac{1}{m^*} = \frac{1}{m_e^*} + \frac{1}{m_h^*}\right)$. For this reason, the energy gap has different values depending on the dot size. By applying Bohr's law in this case, the photon energy for each size has unique value, where it increases as the dot size decreases (*blue shifting*). In fact, the origin of quantum confinement is known to arise from the spatial confinement of carriers within the quantum dot boundary [97]. This means that the spatial confinement coexists with the quantum confinement. Since the spatial confinement of carriers inside a quantum dot is the reflecting or the folding of phonons in the k-space when the dot size decreases, the energy levels will shift to higher (lower) magnitude for conduction (valence) band by the quantum confinement. This relaxes the k-conservation requirement and creates a quasi-direct band gap. Fig.(3-14a) illustrates the effect of spatial confinement for different sizes of the dots. It is noted, that the energy gap does not change, while Fig.(3-14b) indicates the effect of both confinements (spatial and quantum) for the same sizes of dots. Fig. (3-14b) indicates also the widening of the energy gap for different sizes of the dots.

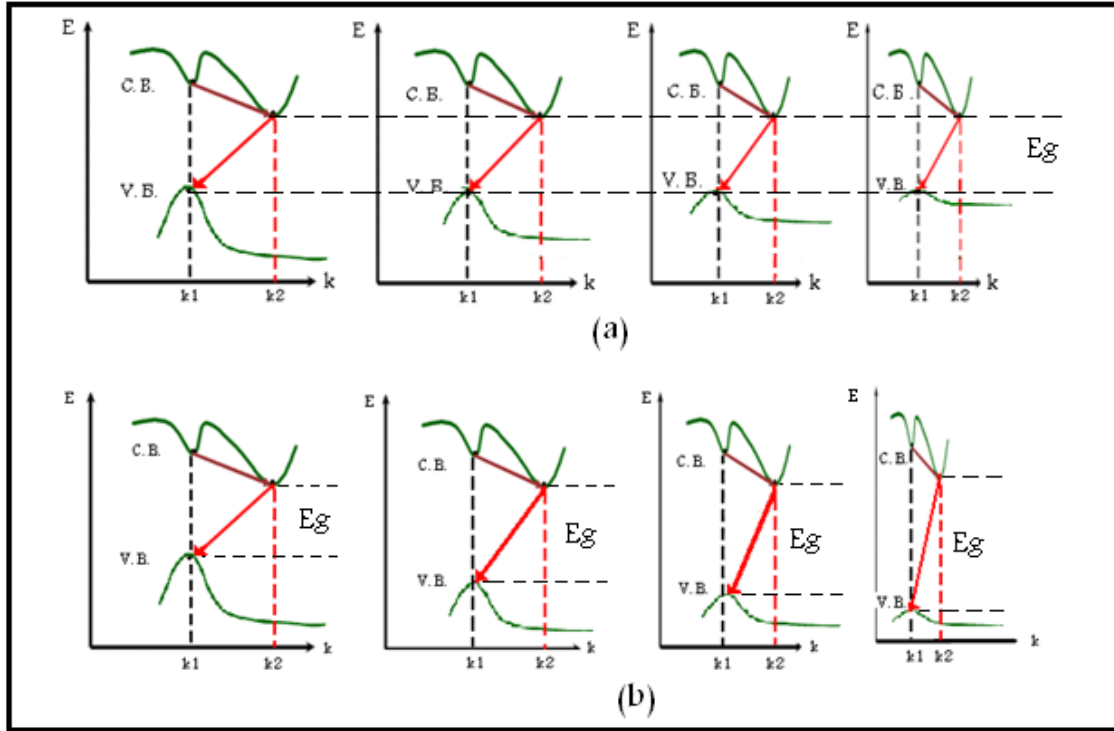


Fig.(3-14): From left to right: (a) the effect of spatial confinement with the decreasing of the dot size. (b) the effect of both spatial and quantum confinement with the decreasing of the dot size [94].

3.6 Conclusions

In this work, a-Si light emitting diode quantum dots are designed. The most important conclusions from this work are:

The quantum confinement's effect occurs in a-SiQDs structure. At room temperature, the internal quantum efficiency shows more efficient than temperature 200 k.

The quantum confinement makes to shift the photoluminescence into visible region (blue shift) by controlling the dot size of a-SiQDs. From this behavior and the quantum efficiency, it is led to the performance that the a-SiQDs material has been changed to be direct band gap material.

In fact, it is difficult to inject electrical carriers into a-SiQDs through the insulating silicon nitride film, although a-SiQDs embedded in silicon nitride

film, so to increase the internal quantum efficiency Ni/Au contact was put on silicon nitride containing a-SiQDs in an attempt to improve the injection current.

The internal quantum efficiency increases with decreasing the injection current, and readily decreases when injection current increases.

The temperature and recombination lifetime affect the quantum efficiency.

The quantum dots size, affects the internal quantum efficiency, since, whenever the dot sizes decrease the quantum efficiency increases and vice versa.

3.7 Suggestions for Future Work

1. Theoretical study on external quantum efficiency for a-SiQDs structure.
2. Light emission from a-SiQDs LED structure is expected to improve the performance at a certain optimum injection current.
3. Light emission from a-SiQDs nanostructure imbedded in carbon matrix.

References

References

1. M. S. Tyagi, "Introduction to Semiconductor Materials and Devices" (John Wiley & Sons 1991).
2. E. F. Schubert, "Light-Emitting Diodes" (Cambridge University Press, Cambridge UK 2003).
3. S. M. Sze, "Semiconductor Device Physics and Technology" 3th edition, Jhon Wiley& Sons, Inc. (2007).
4. Manfred Helm, Thomas Dekorsy, "Silicon Based Microcavity Enhanced Light Emitting Diodes", **143**, pp; 28-29 (2009).
5. N. Zheludev, Nature Photonics **1**, 189 (2007).
6. J.Cooper and T. Cass, Biosensore: A Practical Approach, Oxford University, Oxford, 2004.
7. S. Nakamura, Microelectronics Journal, **25**, 651 (1994).
8. S. Nakamura, M. Senoh, S. ichi Nagahama, N. Iwasa, T. Yamada, T. Matsushita, H. Kiyoku, Y. Sugimoto, T. Kozaki, H. Umemoto, M. Sano, and K. Chocho, Journal of Crystal Growth, **189**, 190 (1998).

9. J.C. Sturm, Y. Huang, L. Han, T. Liu., Phys.Rev.Lett, **25**,509 (2011).
10. W.B. Jackson, S.M Kelso, C.C.Tsai, J.W.Allen, and S.J.Oh, Phys.Rev.B, **31, 6**, 5187(1985).
11. J. Stucke, J. Non-cryst. Sol., **97&98**, 1. ,(1987)
12. J.S.Blackmore, "Solid State physics "Toppan Company, LTD. (2007).
13. T.S.Moss, "Optical Properties of Semiconductores "Academic Press INC., New York, (1995).
14. O.Bisi, S.U.Campisano, L.Pavesi and F.Priolo "Silicon Based Microphotonics: from Basics to Application ‘”**IOS press**, (1999).
15. W. D. A. M. de Boer, D. Timmerman, K. Dohnalová, I. N. Yassievich, H. Zhang, W. J. Buma and T. Gregorkiewicz, Nature Nanotech. **5**, 878–884, (2010).
16. Nidhal Mousa Abdul_Ameer, Moafak Cadim Abdulrida. J. Modren Physics, **2**, 1530 -1537(2011).
17. N. F. MOTT and E. A. DAVISE, "Electronic processes in non-crystalline materials", Oxford University Press, Oxford. (2012).
18. S.J.Fonash "Solar Cell Device Physics", Academic Press, (1981).
19. B.Sapoval, C.Nemamn, "Physics of Semiconductors”, Springer_Verlag New York, (1995).
20. C.M.Wolf, N.Holonyak, and G.E.Stillman, "Pysical Properties of Semiconductores", Prentice Hall International [PHG], (1998).

- 21.** K.Tanaka, E.Moruyama, T.Shimada,and H.Okamoto
"Amorphous Silicon", Jhon Wiley & Sons Ltd. (1999).Translated
by T.Sato.
- 22.** R.A.Street, Hydrogeneted "Amorphous Silicon", Cambridge
University Press, (2005).
- 23.** R. T. Senger and K. K. Bajaj, Phys. Rev., **B 68**, pp: 045313-1-
045313-8, (2003).
- 24.** P. W. Cyr, M.Tzolov, M.A. Hines, I. Manners, E. H. Sargent and
G. D. Scholes, J.Matter.chem. **13**, pp: 2213-2219, (2003).
- 25.** J. S. Williams, R.G. Elliman, H. H. Tan, P. Lever,J.Wrong-Leung
and C. Jagadish, Materials Forum, **26**, pp:74-80,(2002).
- 26.** U. Banin, J.C. Lee, A.A. Guzelian, A.V. Kadavanich, and A.P.
Alivisatoa, Sience Direct, **22, No. 4**, pp: 560-567, (2004).
- 27.** Y. Xia, P. Yang. Sun, Y. Wu, B. Mayers, B. Gates, Y. yin, F. Kim,
and H.Yan, Adv. Mater.**15,No.5**, pp:353-389,(2003).
- 28.** National science and Technology council, "Environmental, Health,
and Safety Research Needs For Engineered Nanoscale Materials",
Executive Office of the president of the United States, September
(2006).
- 29.** F. Charra and S. Gota-Goldmann, "Mesoscopic and Nanostructured
Materials", Part5, Springer Berlin Heidelberg, (2005).
- 30.** C. Kittle"Introduction Solid State Physics", 8th edition, John &
Wiley, (2004).
- 31.** O. Bisi, S. U. Campisano, L. pavesi and F. Priolo "Silicon Based
Microphotonics: from Basics to Applications", IOS Press, (1999).

- 32.** A. Irrera, Ph.D. Thesis, "Light Emitting Device based on Silicon Nanostructures "Universita Degli Studi Di Catania, Italia (2003).
- 33.** Tsui, D. C., H. L. Stormer, J. C. M. Huang, J. S. Brooks, and M. J. Naughton, Phys. Rev., **B28**, 3 (1983).
- 34.** R. B. Phys. Rev. Lett. **50**, 1395 (1983).
- 35.** R. V. Romanujan, Sadhana, **28**, parts 1&2, pp: 81-96, (2003).
- 36.** G. Schmid. M. Decker, H. Ernst, H. Fuchs, and W. Grunwtso, "Small Dimensions and Materails Properties A Definition of Nanotechnology " Europaische Akadamic, November (2003).
- 37.** S. Astilean, Romanian Reports in Physics, **56**, 3, pp: 340-345 (2004).
- 38.** T. H. F. T. e. a. Oosterkamp, **395**, pp: 873-876, (1998).
- 39.** E. Bennici, Ph.D. Thesis, "Amorphous Silicon based Photonic Crystals", university di Macerata, Italia, (2003).
- 40.** M. Dippel, A. Maier, V. Gimple, H. Wider, W.E. Evenson, RL.Rasera, and G. Schaiz, Phys.Rev. Lett. **87**, **No.9**, pp: 095505-1-8, (2001).
- 41.** C. C. Koch, Rev. Adv. Mater. Sci., **5**, pp: 91-99, (2003).
- 42.** J. V. Barth, G. Costantini, and K. Kern, Nature, **437**, pp: 671-679, (2005).
- 43.** Y. Hung, and C. M .Lieber, Pure Appl. Chem., **76**, **No.12**, pp: 2051-2068 (2004).

- 44.** F. P. J. de Groobe, Ph.D.Thesis, "Multi Exciton in GaAs\AlGaAs Quantum Dot Arreys", Technology Universitait Emdhoven, Nederland (2003).
- 45.** J. Koga, K. Nishio, T.Yamaguchi, and F.Yonezawa, Journal of the Physics Social of Japan, **70**, 8, pp: 2478-2484, (2001).
- 46.** J. Koga, K. Nishio, T.Yamaguchi, and F.Yonezawa, Journal of the Physics Social of Japan, **70**, 10, pp: 3143-3148, (2001).
- 47.** F. Yonezawa, K.Nishio, j.Koga, T.Yamaguchi, Journal of The Optoelectronics and Advanced Materails, **4**, **No.3**, pp: 569-574, (2002).
- 48.** C. J. Murphy and J. L. coffer, Focal Point, **56**, **No.1**, p:16A-26A, (2002).
- 49.** M. Rontani, Ph. D. Thesis, "Electronic State in Semiconductor Quantum Dots "Universita Degli Studi Di MODENA, Italia, (1999).
- 50.** T. F. Jiang, X. Tong, and S. Chu, Phys. Rev. **B**, **63**, pp: 045317-1045317-9, (2001).
- 51.** Y. Alhassid, Rev. Mod. Phys., **72**, 4, pp: 895-968, (2000).
- 52.** T.Toyama, Y.Nakai, A.Asano, and H.Okamoto, Journal of Nanocrystalline Solid, **88**, 299-302, (2002).
- 53.** I. Sychugov, R.Juhasz, A.Galechas, J.Valenta, and J.Linnros, Optical Materials, **27**, pp: 973-979, (2005).
- 54.** J. Dian, J.Valenta and J. Hala, J. Appl. Phys., **86**, 3, pp: 1415-1419, (1999).

- 55.** K. Nishio J. Koga, T. Yamaguchi, and F. Yonezawa, *Journal of Nanocrystalline Solid*, **312-314**, pp: 323-326, (2002).
- 56.** K. Nishio J. Koga, T. Yamaguchi, and F. Yonezawa, *Phys. Rev. B*, **67**, 195304-1-195304-5, (2003).
- 57.** H. S. Kwach, Y. Sun, Y. H. Cho, N. M. Park, *Appl. Phys. Lett.* **83**, 14, pp: 2901-2903, (2003).
- 58.** N. M. Park, T. S. Kim, and S. J. Park, *Appl. Phys. Lett.*, **78**, 17, pp: 2575-2577, (2001).
- 59.** N. M. Park, C. J. Choi, T. Y. Seong, and S. J. Park. *Phys. Rev. Lett.*, **86**, 7, pp: 1355-1357, (2001).
- 60.** H. G. Grimmeiss and H. Scholz, "Efficiency of Recombination Radiation in Gap," *Phys. Lett.*, **8**, 233 (2011).
- 61.** D. G. Thomas, J. J. Hopfield and C. J. Frosch, *Phys. Rev. Lett.*, **15**, 857 (2001).
- 62.** C. Godet, B. Equer, D. Mencaraglia, I. Solomon, M.-L. Theye, S. Vignoli, *Nature Photonics*, **7**, pp: 407-412, (2013).
- 63.** Overbys, Dennis, "Nobel Prize in Physics". *New York Times.*, (2014).
- 64.** G. G. Qin, A. P. Li, B. R. Zhang, and B. C. Li, *J. Appl. Phys.* **78**, 2006 (1995).
- 65.** K. D. Hirschman, L. Tsybeskov, S. P. Duttagupta, and P. M. Fauchet, *Nature – London*, **384**, 338 (1996).
- 66.** L. Rebohle, J. von Borany, R. A. Yankov, W. Skorupa, I. E. Tyschenko, H. Fröb, and K. Leo, *Appl. Phys. Lett.* **71**, 2809 (1997).

- 67.** S. Fujita and N. Sugiyama, *Appl. Phys. Lett.* **74**, 308 (1999).
- 68.** N. Lalic and J. Linnros, *J. Lumin.* **80**, 263 (1999).
- 69.** G. Franzò, A. Irrera, E. C. Moreira, M. Miritello, F. Iacona, D. Sanfilippo, G. Di Stefano, P. G. Fallica, and F. Priolo, *Appl. Phys. A: Mater. Sci. Process.* **74**, 1 (2002).
- 70.** J. Valenta, N. Lalic, and J. Linnros, *Opt. Mater. - Amsterdam, Neth.* **17**, 45 (2001).
- 71.** N. M Park, T. S. Kim, and S. J. Park, *Appl. Phys. Lett.* **78**, 2575 (2001).
- 72.** N. M. Park, C. J. Choi, T. Y. Seong, and S. J. Park, *Phys. Rev. Lett.* **86**, 1355 (2001).
- 73.** N. M. Park, S. H. Kim, G. Y. Sung, and S. J. Park, *Chem. Vap. Deposition*, **8**, 254 (2002).
- 74.** T. W. Kim, C. H. Cho, B. H. Kim, and S. J. Park, *Appl. Phys. Lett.* **88**, 123102 (2006).
- 75.** T. Toyama, Y. Kotani, H. Okamoto, and H. Kida, *Appl. Phys. Lett.* **72**, 1489 (1998).
- 76.** P. Anikeeva, J. Halpert, M. Bawendi, V. Bulovic, *Nano Letters*, **9(7)**, 2532–2536, (2009).

- 77.** Seth Coe; Wing-Keung Woo; Mounji Bawendi; Vladimir Bulovic, *Nature*, **420** (6917): 800–803 (2002).
- 78.** Tetsuo Tsutsui "A light-emitting sandwich filling". *Nature* **420** (6917): 753–755, (2002).
- 79.** Nae-Man Park and Gun Yong Sung, *Appl. Phys. Lett.*, **89**, 063509, pp; 063509-3 (2006).
- 80.** Walter P. Murphy, *Appl. Phys. Lett.*, **105**, 121104 (2014).
- 81.** Benjamin S. Mashford, *Nature Photonics*, **26**, 442 (2010).
- 82.** ”, Irati Ugrat, Ivan Castello, Emilio Palomares, Roberto Pacios “Quantum Dots- A Variety of New Applications”, Dr. Ameenah Al-Ahmadi, Ch 6 (2012).
- 83.** Spanier, J. and Oldham, K. B. "The Dirac Delta Function” Ch. 10 in an *Atlas of Functions*. Washington, DC: Hemisphere, pp: 79-82, (1987).
- 84.** Arfken, G., “Mathematical Methods for Physicists”, 3rd ed. Orlando, FL: Academic Press, pp. 481-485 (1985).
- 85.** Omar Manasreh, “Semiconductor Heterojunction and Nanostructure”, McGraw-Hill, (2005).
- 86.** E. F. Schubert, “light-emitting diodes”, (Camberidge University Press, Camberidge, UK 2003).
- 87.** J. M. Martinez-Duart, R. J. Martin-Palma and F. Agullo-Rueda “nanotechnology for Microelectronics and Optoelectronics” Elsevier B. V. , AE Amsterdam, The Netherlands, [2006].

- 88.** D. Denmark, A. Udea, C. L. Shao, M. H. Wu, R. Mu, C. W. White, B. Vlahovic, Solide State Communications, **127**, pp: 463-467 (2003).
- 89.** A. D. Dinsmore, D. S Hus, S. B. Qadri, J. O. Cross, T. A. Kennedy, H. F. Gray, and B. R. Ratna, J. Appl. Phys. **88**, **NO. 9**, pp: 4985-4993 (2000).
- 90.** G. Allan, C. Delerue, and M. Lannoo, Appl. Phys.Lett. , **71**, **NO. 9**, pp: 1198-1191 (1997).
- 91.** B. - H. Kim, C. - H. Cho, T.-W. Kim, N.- M. P ark, G.- Y. Sung, and S. Park, Appl. Phys. Lett, **86**, pp: 091908-1-091908-3, [2005].
- 92.** J. M. Perez, J. Villalobs, P. McNell, J. Prasad, R. Cheek, and J. Kelber, Appl. Phys. Lett., **61**, **No. 5**, pp: 563-565 [1992].
- 93.** Ho-Song Kwack, yuanping Sun, Nae-Man Park and Yong-Hoon Cho., Appl. Phys. Lett., **83**, **No. 14**, pp: 2092-2093 [2003].
- 94.** Nidhal Moosa Abdul-Ameer AL-zubaidi, "Theoretical Investigation of Light Emission From a-Si QDs Nanostructures", Ph.D. University of Baghdad (2010).
- 95.** T.-W. Kim, C.-H. Cho, B.-H. Kim and S.-J. Park, Appl. Phys. Lett., **88**, pp: 123102-1-123102-3, (2006).
- 96.** Hongping Zhao, Guangyu Liu, Jing Zhang, Ronald A. Arif, and Nelson Tansu, Journal of Display Technology, **9**, **No. 4**, (2013).
- 97.** M.Zhou, and I.Ghosh, Piptide Science, **88**, **NO. 3**, pp: 325-339 (2006).

Appendix

Mathcad 2010 Professional Microsoft

©2010 Mathcad, Inc.

www.Mathcad.com

For Finding:

- **The Energy Gap**

$$E_i = 1.56 + \frac{13.9}{d_i^2}$$

$$i = (1:10)$$

$$d_i = (i.1)$$

- **The Injection Current**

$$I_i = 2.6609 - 0.088105 \cdot VD_i + 0.3668 \cdot (VD_i)^2$$

$$VD_i = i. 0.3$$

- **The Wavelength**

$$\lambda_i = \frac{12400}{E_i}$$

- **The Internal Quantum Efficiency**

$$\eta_{\text{int}} = \Phi_{\text{ph}} \cdot \frac{e^{E_i/KT}}{I_{\text{inj}}}$$

$$K_B = 8.61 \cdot 10^{-5}$$

$$T = (200, 300) \text{ k}$$

$$\Phi_{\text{ph}} = 2 \cdot e \cdot \frac{10^{-27}}{\tau_r}$$

$$\tau_r = (11 \cdot 10^{-6} \text{ sec}, 40 \text{ nsec})$$

$$e = 1.6 \cdot 10^{-19}$$

$$i = 1: 10$$

$$d_i = i \cdot 1 \text{ in nm}$$

$$KT1 = 8.61 \cdot 10^{-5} \cdot 300 \text{ in eV}$$

$$T2 = 8.61 \cdot 10^{-5} \cdot 2200 \text{ in eV}$$

$$\tau_{r1} = 40 \text{ in nsec}$$

$$\tau_{r2} = 11 \cdot 10^{-6} \text{ in sec}$$

$$q = 1.6 \cdot 10^{-19} \text{ in C}$$

$$E_i = 1.56 + 13.9 / (d_i)^2 \text{ in eV}$$

$$I_i = 2.6609 - 0.088105 VD_i + 0.3668 (VD_i)^2$$

$$\eta_i = \Phi_{ph} \cdot \frac{e^{E_i / KT}}{I_i}$$

$$\Phi_{ph} = 2 \cdot q \cdot 10^{-27} \tau_r$$

الخلاصة

في هذه الدراسة أستخدمت الحسابات النظرية لنبيطة ثنائي الباعث للضوء للنقاط الكمية من السيليكون العشوائي. وعن طريق هذه الحسابات فقد تبيننا فكرة التقييد الكمي. وقد وجد ان الانبعاث الكمي الضوئي يُظهر اعتمادا مهما لحجم النقاط الكمية والتي تتراوح من (1-4) نانومتر. إن الكفاءة الكمية الداخلية تتأثر بدرجة الحرارة حيث تكون اكثر كفاءة عند درجة حرارة الغرفة. يمكن لفجوة الطاقة ان تتناغم وفقا للتحكم بحجم النقاط الكمية من السيليكون العشوائي. وقد اظهرت النتائج الازاحة نحو الطاقا العاليه في تأثير حالة التقييد الكمي، لهيكل النقاط الكمية للسيليكون العشوائي. وهذا التقييد الكمي يجعل السليكون مرشح للعرض بكامل ألوان الطيف البصري. مما يقودنا هذا السلوك البصري الى تفسير تغير مادة النقاط الكمية للسيليكون العشوائي لتصبح مادة ذات فجوة حزمية مباشرة بعد ان كانت غير مباشرة في طبيعتها الحجمية. تمت دراسة الكفاءة الكمية الداخلية بوصفها دالة الى الطول الموجي وتيار الحقن. لقد وجدنا ان النتائج المستحصلة متفقه اتفاقا جيدا مع النتائج التجريبية المنشورة. لذا، فاننا نوكد على ان مادة النقاط الكمية من السليكون العشوائي هي خيار واعد لنبائط أنبعاث الضوء المرئي والقابلة للتناغم الطاقوي وذات انجازية عاليه



جمهورية العراق
وزارة التعليم العالي والبحث العلمي
جامعة بغداد
كلية التربية للعلوم الصرفة / ابن الهيثم

السليكون العشوائي للثنائي الباعث للضوء من النقاط الكمية

رسالة مقدمة الى

مجلس كلية التربية للعلوم الصرفة / ابن الهيثم - جامعة بغداد
كجزء من متطلبات نيل درجة ماجستير علوم في الفيزياء

من قبل

ولاء خليل جميل خليل

بكلوريوس-2012

بإشراف

د. موفق كاظم عبد الرضا

أستاذ مساعد